phys. stat. sol. (b) **202**, 605 (1997)

Subject classification: 61.80.Jh; 68.35.Bs; 73.40.Ns; S6

A Review of SiC Reactive Ion Etching in Fluorinated Plasmas

P. H. Yih (a), V. Saxena (b), and A. J. Steckl[1]) (b)

(a) Bell Laboratories, Lucent Technologies, Orlando, FL 32819, USA

(b) Nanoelectronics Laboratory, Department of Electrical and Computer Engineering/ Computer Science, University of Cincinnati, Cincinnati, OH 45221-0030, USA

(Received January 31, 1997)

Research and development in semiconducting silicon carbide (SiC) technology has produced significant progress in the past five years in many areas: material (bulk and thin film) growth, device fabrication, and applications. A major factor in this rapid growth has been the development of SiC bulk crystals and the availability of crystalline substrates. Current leading applications for SiC devices include high power and high temperature devices and light emitting diodes. Due to the strong bonding between Si and C (Si–C = 1.34 × Si–Si), wet chemical etching can only be performed at high temperature. Therefore, plasma-based ("dry") etching plays the crucial role of patterning SiC for the fabrication of various electronic devices. In the past several years, reactive ion etching (RIE) of SiC polytypes (3C and 6H) has been investigated in fluorinated gases (primarily CHF_3, $CBrF_3$, CF_4, SF_6, and NF_3), usually mixed with oxygen and occasionally with other additives or in a mixture of fluorinated gases. In this paper, a review of SiC RIE is presented. The primary emphasis is on etching of the 3C and 6H polytypes, but some results on RIE of the 4H polytype are included. The paper covers the basic etching mechanisms, provides typical etching properties in selected plasma conditions, discusses the effects of changes in various etching parameters, such as plasma pressure, density and power, etching time, etc. The etching of features of sizes varying from sub-μm to tens of μm's is addressed. Finally, optimum etching conditions and trade-offs are considered for various device configurations.

1. Introduction

In the early 1960's, at the beginning of modern silicon carbide (SiC) development, SiC research was conducted only on small pieces (<1 cm) produced by the Acheson process [1], which is currently used for the sand paper industry. In the recent years, larger area 6H- and 4H-SiC substrates (reaching ≈5 cm diameter) obtained from boules grown by the modified Lely sublimation method have become commercially available [2]. The availability of these SiC substrates has led to greatly increased research and development in all aspects of SiC. High-quality cubic and hexagonal SiC epitaxial layers have been successfully grown on the crystalline SiC substrates. For useful SiC device production, large area and defect-free [3] substrates are required. At the same time, the growth of 3C-SiC on Si substrates, has continued to improve [4 to 7]. This heteroepitaxial approach has the ultimate goal to provide truly large area and low cost SiC substrate materials, as well as the potential integration of SiC high voltage technology with Si

[1]) The author to whom correspondence on this paper should be addressed.
e-mail: a.steckl@uc.edu

microelectronics. This general material availability has opened the way to significant progress in the fabrication of various SiC electronic devices for applications requiring high-temperature, high-speed, and high-power operation [8 to 13]. Promising electrical performance for MESFET's [14, 15], MOSFET's [16, 17], thyristors [18, 19], non-volatile memory devices [20, 21], heterojunction bipolar transistors (HBT) [22 to 27], charge-coupled devices (CCD) [28], and high breakdown voltage Schottky [29 to 40] and p–n junction diodes [41 to 45] have been reported. Various etching characteristics are required for the patterning of these devices. Reviews [46, 47] of higher power semiconductor electronics show SiC as the best candidate material for the near future smart power technology. This is mainly due to its outstanding material properties such as high thermal conductivity, high electric field breakdown, high electron saturation velocity, and relatively better developed device fabricated processes.

The paramount reason for using plasma-based etching of Si or III–V semiconductor materials is to take advantage of the relative anisotropy of plasma etching in order to precisely control the line-width. This becomes extremely important when the device feature is at the sub-μm scale (<1 μm). For SiC, another important reason to employ plasma etching is the chemical stability of SiC which makes "wet" etching of device structure very difficult. Indeed, wet etching of SiC has to be done either at elevated temperature (>600 °C) in alkaline solutions [48] or with photoelectrochemical etching at room temperature [49 to 51]. It is important to note that line-width control is very difficult in the wet etching of SiC process under such high temperature or photo-assisted chemical etching. This explains why plasma-assisted ("dry") etching plays a crucial role in the fabrication of various of SiC devices, for both large and small dimensions.

Reactive ion etching (RIE) of SiC in fluorinated plasmas has been developed to the point where it is now widely employed in both the research and development environment and commercial product fabrication [2]. In our research laboratory at the University of Cincinnati, we have worked for the past ten years on the RIE of SiC for electronic device fabrication. We have investigated aspects of SiC RIE in fluorine-based plasmas, leading to a greater understanding of dry etching issues of SiC materials. In the early stage of these investigations, amorphous [52] and polycrystalline SiC [53] were employed. More recently, 3C-, 4H- and 6H-SiC RIE have been reported in a variety of fluorinated gases (CHF_3, $CBrF_3$, CF_4, SF_6, and NF_3) usually in combination with oxygen. SiC RIE in fluorinated plasmas has been shown to produce useful etch rates (100 to 1000 Å/min) and a high degree of etching anisotropy leading to the patterning of sub-μm features. One difficult aspect of SiC RIE has been the formation of residues (which lead to a rougher surface) after longer term etching under many conditions. This is (in part) because the commercial RIE systems are designed to accommodate multiple large Si wafers rather than the much smaller SiC substrates currently available (thus the area of the electrode is usually much larger than that of the SiC samples being etched). Residue formation can be a serious problem for subsequent processes, such as metal contact (ohmic or Schottky) formation. Several techniques which have now been successfully developed to prevent residue formation are reviewed in the latter section of this paper. Very limited information has been reported [54] on SiC etching in chlorine-based plasmas, which has the potential for using non-metallic etch mask materials (e.g. SiO_2) and obtaining residue-free etching. SiC etching in fluorine-based high density electron cyclotron resonance (ECR) plasma was reported recently [55, 56] with promising results for high etch rate, anisotropic profile, and residue-free (smooth) surface topography.

In this paper, a review of the current understanding and practice of reactive ion etching of SiC is presented. We concentrate on the fluorine-based RIE of 6H-SiC, the most widely used polytype. However, some results in the plasma-assisted etching of 3C and 4H polytypes are also discussed. The topics include: a) basic plasma etching mechanisms in fluorinated-oxygen mixtures; b) etching characeristics – etch rate (ER), etch aspect ratio (EAR), etch rate ratio (ERR or selectivity) to Si, SiO_2 – and their dependence on plasma parameters (power, pressure, and density); c) techniques for obtaining smooth (residue-free) etched surfaces; d) techniques for etching sub-μm features; e) an introduction to various high density plasma sources; f) a discussion of suggested etching conditions and trade-offs in light of various device configurations. Finally, we discuss the recent progress on high density plasma etching of SiC.

2. Basic Plasma Etching Mechanisms

In this section a brief overview is given of the basic mechanisms at work during reactive ion etching (RIE) of SiC at room temperature. Both physical and chemical processes participate in the overall removal of Si and C atoms of SiC. Basically, all chemical etching processes probably consist of three sequential steps [57, 58]: 1. adsorption of the etching species; 2. product formation; 3. product desorption. During a plasma discharge a variety of species are produced [59]: charged particles (ions and electrons), photons, and neutrals (radicals). Plasma etching of materials can proceed via a combination of physical and chemical mechanisms. The dominant mechanism is determined by the volatility of the reaction by-products and the energy of the ionized species. In practice, this translates into choices regarding the feed gas (inert or reactive), the plasma pressure and the choice of connecting the sample biasing electrode to the RF power or to ground. These conditions result in plasma etching processes which can be grouped into four categories: a) *sputtering* – purely physical removal of the material by energetic ions of the gas molecules; b) *chemical plasma etching* – neutral radicals formed in the plasma react with the substrate material to produce volatile species ; c) *ion-enhanced chemical etching* – energetic ions damage the etch surface, enhancing its reactivity; d) *inhibitor-controlled chemical etching* – ion bombardment removes inhibitor layers from surfaces orthogonal to the ion flux, allowing chemical etching to proceed. Reactive ion etching, which encompasses the last two categories, operates at relatively low pressures (from a few mTorr to hundreds of mTorr) with the sample placed on the cathode, thus resulting in the production of fairly energetic ions along with the formation of reactive radicals. Plasma-based etching in the RIE mode generally allows for the most useful trade-offs between etch rates and anisotropy.

The overall etch rate is given by the combination for the material removing mechanisms outlined above:

$$R = R_{\text{SPUTTER}} + R_{\text{NEUT}} + R_{\text{IEN}} + R_{\text{ICN}}\,, \tag{1}$$

where R_{SPUTTER} is the ion sputter-removal rate, R_{NEUT} is the chemical etching performed by neutral radicals, R_{IEN} is the ion-enhanced neutral chemical etching, and R_{ICN} is the inhibitor-controlled neutral etching. To understand the effect of the arrival rate of ions and neutrals on the overall etch rate, Eq. (1) can be expanded [60 to 62] as follows:

$$R = F_{\text{I}}\varphi_{\text{S}} + F_{\text{N}}(1 - \alpha - \beta)\,\varphi_{\text{N}} + F_{\text{N}}\alpha\varphi_{\text{N}}^{*} + F_{\text{N}}\beta\varphi_{\text{N}}^{**}\,, \tag{2}$$

where F_I is the ion flux (ions/cm^2 s), F_N is the flux of neutral particles, φ_S is the sputtering efficiency (cm^3/ion), φ_N is the chemical etch rate efficiency of neutral species (cm^3/neutral), φ_N^* and φ_N^{**} are the chemical etch rate efficiencies of neutral species on the fraction (α) of the surface which has been ion bombarded ("sensitized") and on the surface fraction (β) covered by an etch inhibitor. The sensitized surface fraction obviously increases with the ion flux. The ion flux also (negatively) affects the inhibitor covered fraction, thus enhancing the chemical (neutral) etch rate. Basically, this model simply explains the relationship between the two major plasma species (neutral radicals and ions) involved in the plasma-assisted ("dry") etching process.

For SiC etching in mixtures of fluorinated gases and oxygen, the most likely chemical reactions associated with the removal of Si and C atoms are given in Eq. (3) to (5) [53], leading to the combined chemical reaction shown in Eq. (6) for the removal of SiC molecules. However, it is assumed that actual molecular removal is unlikely. To some extent, we do not consider the other reaction compounds, such as COF_2, in the following discussion:

$$\mathrm{Si} + m\mathrm{F} \rightarrow \mathrm{SiF}_m \qquad (m = 1 \text{ to } 4)\,, \tag{3}$$

$$\mathrm{C} + m\mathrm{F} \rightarrow \mathrm{CF}_m\,, \tag{4}$$

$$\mathrm{C} + n\mathrm{O} \rightarrow \mathrm{CO}_n \qquad (n = 1 \text{ to } 2)\,, \tag{5}$$

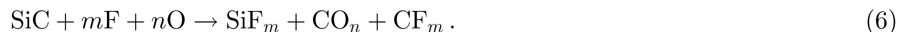

$$\mathrm{SiC} + m\mathrm{F} + n\mathrm{O} \rightarrow \mathrm{SiF}_m + \mathrm{CO}_n + \mathrm{CF}_m\,. \tag{6}$$

In silicon RIE, the presence of oxygen in fluorinated plasma produces important effects, due to several mechanisms [63]. *First*, [O] atoms react with unsaturated fluoride species generating reactive F atoms, while simultaneously depleting these polymer-forming species. *Second,* when increasing O_2 is added to the feed gas, sufficient [O] chemisorbs on the silicon surface making it more "oxide-like", thus reducing the available Si sites for etching. *Third,* if the oxygen additive is introduced as a replacement for the fluorinated gas in order to keep the total flow rate constant, dilution effects reduce the etch rate. The effect of oxygen additive can be readily seen in the etching of Si in $CBrF_3/O_2$, CF_4/O_2, and SF_6/O_2 gas mixtures [53]. The highest etch rate is obtained when a relatively low oxygen (≈5 to 20%) percentage is added to the fluorinated gas to enhance the generation of etchant species and to deplete polymer species. Beyond this point, as the oxygen percentage continues to increase, the etch rate monotonically decreases. A model was proposed for the etching of Si [64, 65]. When Si is exposed to [F] atoms, it acquires a fluorinated skin (fluorine atom adsorption) which extends a few monolayers below the surface. While most [F] atoms involved in the etching process react with the surface, a small fraction attack underlying Si–Si bonds (3.38 eV), liberating SiF_m molecules. In Si etching, the [F/C] ratio, where [C] originates in the gas phase (etchant), was proposed [58] as a determinant of the etching dependence on the process pressure, input power, and additives. A high [F/C] ratio in the gas produces a high etch rate, while at a sufficiently low [F/C] ratio a polymer film could be deposited on the surface during the process, resulting in a negative etch rate or a taper (width of top < bottom) etching profile. Polymer formation could be even more severe when H_2 is present in the plasma. This is a typical example of competition between etching and deposition that determines the etching profile [66].

Turning now to SiC RIE in fluorinated plasmas, the etching process contains both similarities and differences from the Si case. For example, highly anisotropic etching profiles are obtained (>10:1) during the residue-free etching process which employs a

graphite sheet covering the powered electrode [67]. In this case, an [F/C] ratio much smaller than unity is expected, since copious levels of [C] are produced from several sources: the SiC itself, the etchant gas (in the case of fluorocarbons), and most importantly from the graphite sheet. This indicates that the [F/C] ratio model used successfully for Si etching must be modified for SiC etching. For example, an anisotropic etching profile was obtained for SiC in SF_6/O_2 mixtures, which is not the case of normally undercut etching profile for Si [68, 69]. The reason is due to SiC itself providing carbon, which enhances the polymer formation, preventing the side wall from being etched. However, there were no fluorinated gases we have investigated which produced an undercut profile during SiC etching.

In addition to the indirect roles of oxygen in the gas phase reaction, oxygen also participates by directly removing C atoms in SiC through the reaction given in Eq. (5). Carbon can be etched in either a pure fluorine-containing plasma (Eq. (4)) or a pure O_2 (Eq. (5)) plasma. As reported by several research groups [52, 53, 67, 70], a thin carbon-rich layer is formed on the etched surface. This indicates that C is not removed sufficiently fast from the etched surface through the reaction of either carbon−fluorine [C−F] or carbon−oxygen [C−O] reactions. At low (or zero) % O_2, it has been suggested [70] that carbon is preferentially removed through the formation of CF_m (Eq. (4)) rather than $C{-}O_n$ (Eq. (5)), whereas at high O_2% removal of carbon is dominated by the [C−O] reaction. However, generally the SiC etch rate decreases as the O_2 percentage increases. This indicates that the [C−O] reaction through Eq. (5) may not be as efficient as the [C−F] reaction through Eq. (4). This explains why one obtains the highest 3C-SiC etch rate under low oxygen percentage conditions, which produce high fluorine intensity in CF_4/O_2, NF_3/O_2, and SF_6/O_2 mixtures (Fig. 1 to 3), and for higher oxygen percentage (60 to 80%) in CHF_3/O_2.

Along with the purely chemical plasma etching process, the effect of the energetic ion flux needs to be considered. This primarily consists of damage or breaking of the surface Si−C bond (4.52 eV), which enhances the chemical reaction efficiency, and removal of non-volatile surface species, which enables the chemical reaction to proceed. The latter includes providing sufficient energy to break the strong C−C bonding (6.27 eV) that could exist in the C-rich layer. This combination of effects have led to a two regime model for the effect of dc bias on the etch rate of polycrystalline SiC [53]: a) at low dc bias conditions, the low energy (and effectiveness) of the ion flux is the dominant mechanism; b) at sufficiently high values of the dc bias, the ion energy is high enough to no longer limit the process and the etch rate is determined by the removal efficiency of the chemical reaction.

3. Experimental Conditions

In order to draw meaningful conclusions regarding effects of various etching parameters we have mostly utilized a common set of etching conditions in all experiments. This consists of an rf power of 200 W (0.4 W/cm^2), a pressure of 20 mTorr, a total flow rate of 20 sccm, and etch times of 5, 20, and/or 30 min. In the following sections, we refer to these experimental values as the "standard" etching condition. A few exceptions to the standard condition are made: a) for the use of low flow rate (5 sccm) H_2 additive in which case the plasma pressure was increased by 5 mTorr to minimize the reactant-limited effect; b) for evaluating mixtures of NF_3/SF_6 where a flow rate as high as 35 sccm was utilized. Several other research groups also reported on the RIE etching of SiC in a

variety of conditions. Usually, they operated at a much higher etching pressure, ranging as high as 200 mTorr, or in a microwave plasma. The process pressure plays a critical role in determining the value of the dc bias (ion energy), the etchant species lifetime (reciprocal to pressure), macro- and micro-uniformity, and the level of polymer formation. Unfortunately, in many cases, there is not sufficient information on the etch rate for a meaningful comparison. However, relevant data from other groups is discussed and referenced in separate sections (Sections 4.3, 5.3.2 and 6).

To quantitatively measure the relative intensity of the primary plasma species, a computer controlled optical emission spectrometer (OES) monitored the photoemission from the plasma during the process. The dc bias and plasma species intensity were recorded after striking the plasma for 1 min. Noble gas actinometry [71] was regularly employed, using 0.6 sccm (3% of total gas flow rate) of Ar added to the gas feed, to obtain the relative concentration of various species, such as [H], [F], [Ar], [O], and [Br]. Plasma photoemission was monitored at wavelengths of 486 nm for hydrogen [H], 703 nm for [F], 750 nm for argon [Ar], 777 nm for oxygen [O], and 336 nm for bromine [Br].

Several categories of SiC material were utilized for our etching experiments: a) *3C-SiC*: 6 to 8 μm unintentionally doped n-type layers grown on p-type Si(100) by conventional chemical vapor deposition [4]; b) *6H-SiC*: primarily n-type (0001) Si-face substrates [2] with doping concentration of 10^{17} cm^{-3}; in one set of experiments: n^{+} substrates with doping concentration of 10^{19} cm^{-3}, and p-type substrates with doping concentration of 10^{18} cm^{-3}; c) *4H-SiC*: n-type (0001) Si-face substrates [2] with doping concentration of 9.9×10^{18} cm^{-3}. Sputter deposited aluminum patterned by lift-off process was employed as the etch mask. The Al metal mask was removed prior to measuring the etch step height (and associated etch rate) and surface analysis. The step height was measured with a surface profilometer (Dektak). Generally, the sample size was kept small enough so that it does not significantly influence the nature of the discharge during the process. This is extremely important for the comparison of experiments with the same nominal etching condition.

4. Etching in Fluorinated Gas Mixtures

As discussed in Section 2, the RIE of SiC is performed in a primary fluorinated gas to which secondary gases (oxygen and hydrogen) may be added to control or enhance the process. In the work reviewed here, the primary gas consists of one of the following gases: CF_4, SF_6, NF_3, $CBrF_3$, and CHF_3. Mixtures of certain fluorinated gases were also investigated. The reasons for choosing these gases are given below along with their etching characteristics. Other characteristics frequently investigated include the etching anisotropy (through the line edge profile) and the density of residues in the etch field. The most important characteristic to be measured is, of course, the etch rate. In addition, plasma characteristics, such as the self-induced bias and the density of the main plasma species (such as [F], [O], [H]), are normally measured in order to understand the mechanisms determining the process. Finally, the process parameter most commonly varied is the level of the secondary gas.

4.1 Fluorinated-oxygen mixtures

In this section, we review the important characteristics of 3C-SiC etching in mixtures of fluorinated gases and oxygen and compare 3C- and 6H-SiC RIE. In all experiments de-

scribed below, the standard etching conditions mentioned before, with an etch time of 5 min were employed. The SiC samples were unintentionally-doped n-type 3C-SiC grown on p-type Si [4], with the exception of RIE in $CBrF_3/O_2$ mixture where high temperature annealed polycrystalline 3C-SiC sputter deposited on Si was employed [53]. Si and SiO_2 (thermally grown) samples were also etched simultaneously with 3C-SiC samples, to provide the etch rate ratios (ERR) of SiC/Si and SiC/SiO_2 required for fabrication of SiC/Si heterojunction devices, such as HBT. The 6H-SiC samples were n-type Si-face (0001) commercially available [2] substrates. The 3C-SiC etching characteristics (etch rate, ERR and relative density of main etching species) are shown in Figs. 1 to 5 for CF_4, SF_6, NF_3, CHF_3, and $CBrF_3$ as a function of O_2%. Fig. 6a shows the comparison of the etch rates obtained using each of these gases on the same plot. The self-induced dc bias resulting in the various etching conditions is shown in Fig. 7. Some of the main conclusions regarding 3C-SiC RIE are: a) a relatively high etch rate can be obtained in SF_6/O_2 and NF_3/O_2 mixtures; b) a high SiC/Si ERR is produced in low fluorinated gases, such as CHF_3/O_2 and $CBrF_3/O_2$ mixtures; c) the dc bias is not a portable parameter; d) highly anisotropic etching profile can be obtained in all fluorinated oxygen plasmas except CHF_3/O_2 mixtures. Details of the etch aspect ratio for these cases were reported elsewhere [53] and will not be repeated here.

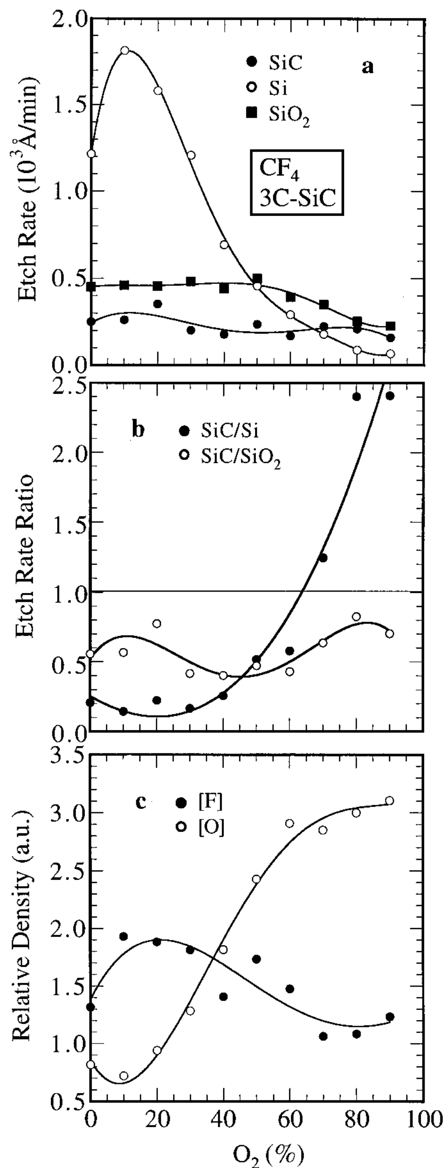

Fig. 1. 3C-SiC RIE in CF_4 as a function of O_2 plasma under the standard conditions a) SiC, Si, and SiO_2 etch rate, b) SiC/Si and SiC/SiO_2 etch rate ratio under the standard conditions, c) relative [F] and [O] densities [73] (a.u. means arb. units)

4.1.1 3C-SiC etching in CF_4/O_2 [52, 67, 70, 72 to 76]

CF_4 was one of the first halogens used for plasma-assisted etching [58, 61] and its characteristics in etching Si are well-known [63]. The SiC, Si, and SiO_2 etch rates in CF_4/O_2 mixtures and related information are given in Fig. 1. The typical effect of the O_2 percentage

on the Si etch rate is observed, with the etch rate experiencing a sharp maximum ($\approx 1.8 \times 10^3$ Å/min) in the vicinity of the peak in the [F] concentration in the plasma ($\approx 10\%$ O_2) and then decreasing rapidly with increasing O_2 percentage. The SiC etch rate exhibited a much less pronounced peak value of 350 Å/min at 20% O_2. No effect of O_2 percentage on the SiO_2 etch rate (≈ 450 to 500 Å/min) was observed in the 0 to 50% range. At higher O_2 levels, the SiO_2 etch rate slowly decreases and reaches a low value of ≈ 210 Å/min at 90% O_2. ERRs of SiC/Si and SiC/SiO_2 are shown in Fig. 1b. An ERR > 1 for SiC/Si is obtained at high (70 to 90%) O_2 percentage, where its effect is more pronounced on the Si etch rate than on the SiC etch rate. No ERR > 1 for SiC/SiO_2 was found in the entire range of O_2 percentage. As shown in Fig. 1c, the [F] and [O] plasma emission intensities were monitored as the main etching species, thus providing a measure of their relative density in the plasma. As expected, the [F] intensity experiences a maximum at a relatively low level of O_2 in the gas stream, whereas the [O] intensity increases monotonically with the O_2 percentage. A cross-over point between the [F] and [O] intensities is observed at $\approx 40\%$ O_2. As noted by other workers in the field [53], the pattern of the Si etch rate with O_2 percentage shows at first a strong increase due to additional [F] liberated by oxygen, followed by eventual reduction due to the dilution effect. On the other hand, no such strong relationship was found between the SiC etch rate and the [F] and/or [O] emission intensities.

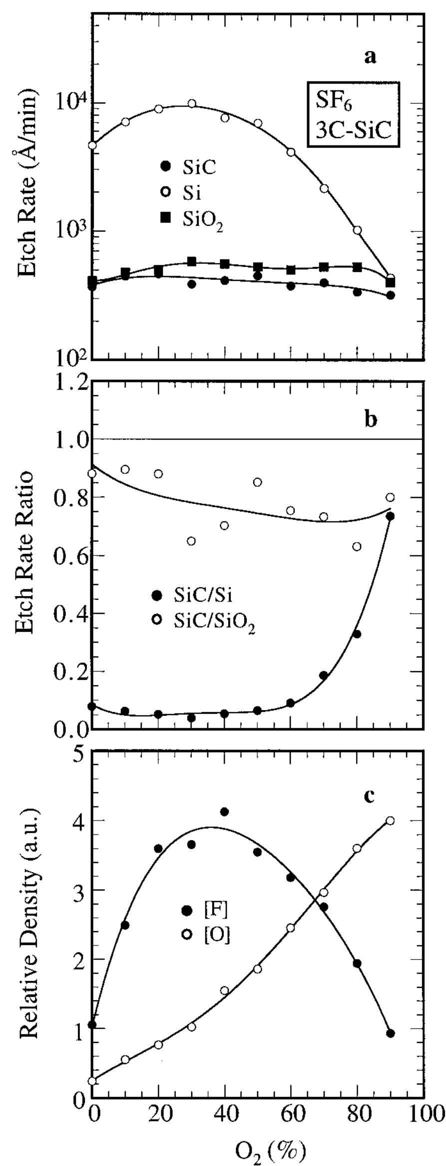

Fig. 2. 3C-SiC RIE in SF_6 as a function of O_2 plasma under the standard conditions a) SiC, Si, and SiO_2 etch rate, b) SiC/Si and SiC/SiO_2 etch rate ratio, c) relative [F] and [O] densities [3]

4.1.2 3C-SiC etching in SF_6/O_2 [53, 73, 75 to 78]

The abundance of [F] in the SF_6 plasma produces a high Si etch rate, which is particularly favorable for applications requiring etching of thick layers such as micromachining [68] and power device patterning [69]. Re-

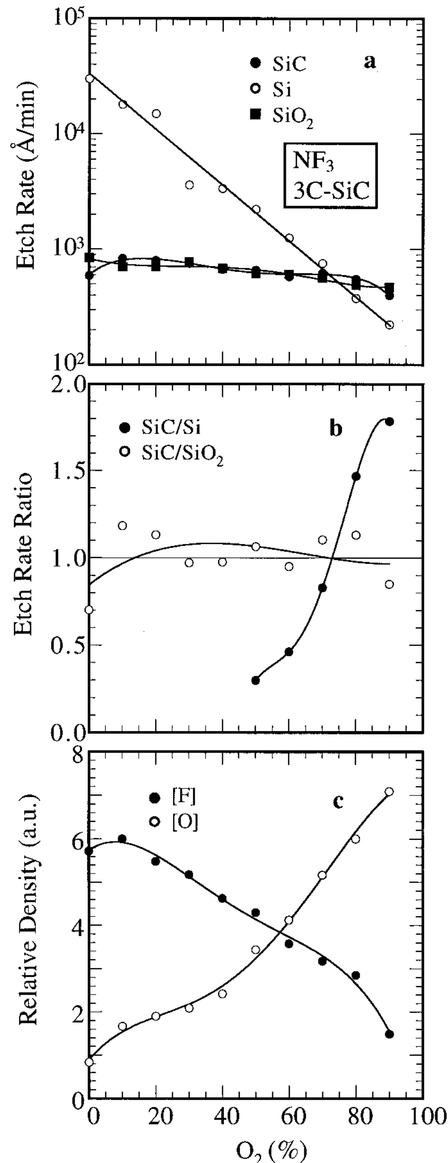

Fig. 3. 3C-SiC RIE in NF_3 as a function of O_2 plasma under the standard conditions a) SiC, Si, and SiO_2 etch rate, b) SiC/Si and SiC/SiO_2 etch rate ratio, c) relative [F] and [O] densities [73]

garding SiC etching, SF_6 does not provide a source of C in the gas phase, unlike CF_4. Results obtained in etching of SiC, Si, and SiO_2 in SF_6/O_2 mixtures are shown in Fig. 2. The Si etch rate follows the same trend as the [F] concentration as a function of O_2%, reaching a maximum of 9×10^3 Å/min at 30% O_2. By comparison, the SiC and SiO_2 etch rates are nearly constant with O_2 percentage. The highest SiC etch rate (≈450 Å/min) is obtained at 20% O_2. ERRs of SiC/Si and SiC/SiO_2 are shown in Fig. 2b. No etch selectivity greater than unity was found for either SiC/Si or SiC/SiO_2 within the full range of O_2 percentage. SF_6/O_2 is the only gas mixture reported in this paper which shows no ERR > 1 for either set of materials. As shown in Fig. 2c, a cross-over point of [F] and [O] emission intensities is present at ≈70% O_2. No simple relationship was found between either [F] or [O] emission intensity and the SiC etch rate.

4.1.3 3C-SiC etching in NF_3/O_2 [67, 73, 75, 78]

NF_3 is perhaps the most copious producer of [F] species in the plasma, hence resulting in very high Si etch rates [73]. With regard to SiC etching, NF_3 like SF_6 is not a source of C, but unlike SF_6 it produces only volatile by-products. Etching results for SiC, Si, and SiO_2 in NF_3/O_2 mixtures are given in Fig. 3. The Si ER is highest (≈3 μm/min) in pure NF_3 and drops exponentially with the addition of O_2. In sharp contrast, the SiC and SiO_2 ERs experience neither a tremendous etch rate in pure NF_3 nor a rapid decrease with O_2 dilution. Nearly equal ERs of SiC and SiO_2 were obtained in the full range of O_2 percentage. The highest SiC etch rate of ≈830 Å/min was obtained at 10% O_2. Etch selectivities of SiC/Si and SiC/SiO_2 shown in Fig. 3b indicate that a SiC/Si ERR greater than unity is obtained at high O_2 percentage (>70%). The [F] and [O] plasma emission intensities in NF_3/O_2 mixtures are shown in Fig. 3c. Among the gas mixtures investigated, NF_3/O_2 plasmas produce the

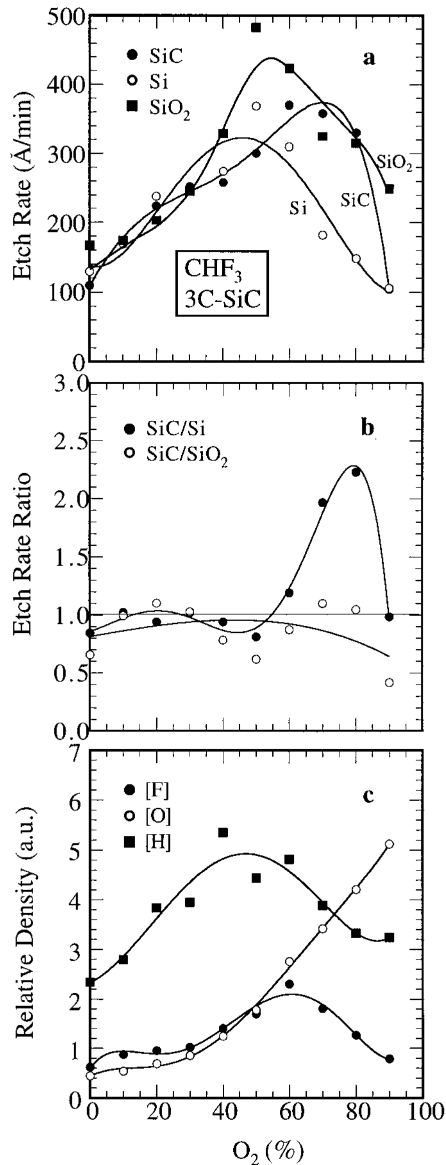

Fig. 4. 3C-SiC RIE in CHF_3 as a function of O_2 plasma a) SiC, Si, and SiO_2 etch rate, b) SiC/Si and SiC/SiO_2 etch rate ratio, c) relative [F], [O], and [H] densities [73]

highest [F] emission levels. Highly anisotropic SiC etching profile in NF_3/O_2 mixture was reported in detail elsewhere [73]. The [F] emission intensity decreases linearly as a function of O_2 percentage so that O_2 plays a role of diluent. A cross-over point of [F] and [O] emission intensity was obtained at ≈60% O_2.

4.1.4 3C-SiC etching in CHF_3/O_2 [53, 73, 75]

While not an obvious choice, CHF_3 is an interesting gas for etching SiC. By comparison to CF_4, in CHF_3 one of the F atoms is replaced with H. This significantly reduces the [F] density since hydrogen also acts as a scavenger for [F]. In turn, as shown in Fig. 4, this greatly decreases the Si etch rate at low O_2 percentage, but does not significantly affect the SiC etch rate. At the same time the presence of [H] in the plasma has the important positive effect of reducing the density of residues present in the etch field (see discussion in Section 5). The highest SiC etch rate of ≈370 Å/min was obtained at 60% O_2 plasma, while the highest Si and SiO_2 etch rates of 370 and 480 Å/min were both obtained at 50% O_2. Beyond the 50% O_2 level, the effect of increasing O_2 percentage is to rapidly decrease the Si etch rate, while the SiC etch rate still increases up to the 60% O_2 level and then decreases slowly until the 80% level is reached. A SiC/Si ERR > 1 was obtained in the range of 60 to 80% oxygen, with the highest ERR of ≈2 being obtained at 80% O_2. Interestingly, the etch rates of SiC and SiO_2 exhibit similar trends with oxygen percentage, resulting in a SiC/SiO_2 ERR of 0.5 to 1.0 over the entire range of CHF_3/O_2 mixtures. Since the effect of the dc bias (see Fig. 6) in increasing the etch rate is probably stronger for Si than SiC, the fact that the SiC/Si ERR increases with O_2 in the 60 to 80% range indicates the dominance of the C–O chemical reaction. The [F], [O], and [H] plasma emission intensities are shown in Fig. 4c. It is interesting to note that the same cross-over point of 50% O_2 was obtained for the [F] and [O] relative concentrations and for the SiC and Si etch rates (Fig. 4b). Of

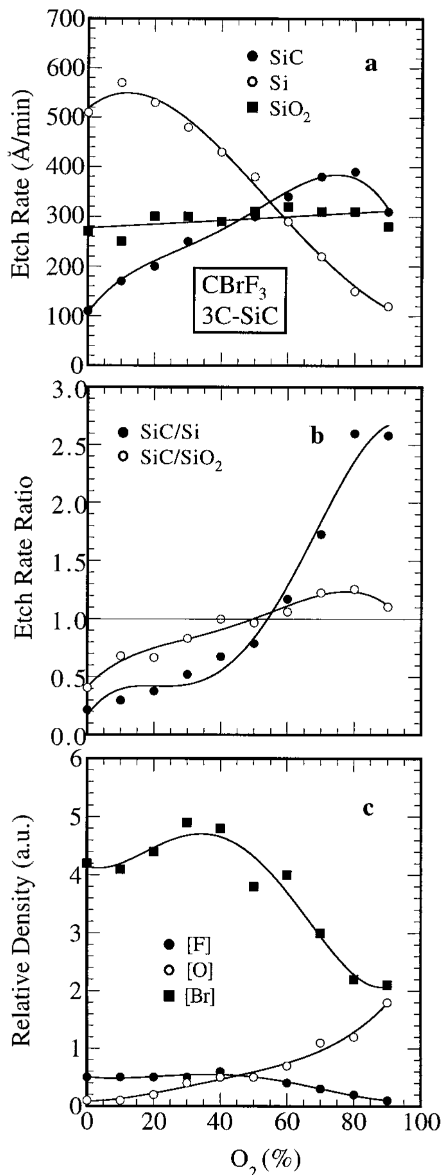

Fig. 5. Polycrystalline 3C-SiC RIE in $CBrF_3$ as a function of O_2 plasma a) SiC, Si, and SiO_2 etch rate, b) SiC/Si and SiC/SiO_2 etch rate ratio, c) relative [F], [O], and [Br] densities [53]

course, at high enough O_2 percentage the [F] level decreases to the point where it becomes the rate limiting step in the etching process and the SiC etch rate drops off very quickly. Therefore, multiple effects, involving the [F], [O], and [H] intensities (and the dc bias level) combine to control the reactive ion etching process of SiC.

4.1.5 3C-SiC etching in $CBrF_3/O_2$ [53]

The last etching gas to be discussed, $CBrF_3$, is the only one investigated which combines two different halogen atoms in a single molecule. By comparison to CF_4, in $CBrF_3$ one of the F atoms is replaced with Br. The results of etching polycrystalline 3C-SiC in $CBrF_3/O_2$ plasma are shown in Fig. 5. The Si ER pattern as a function of O_2 percentage is similar to that observed for CF_4 (see Fig. 1) but with much lower ER values. For example, the peak CF_4 ER of $\approx 1.8 \times 10^3$ Å/min which occurs at 10% O_2 is three times higher than the peak ER of ≈ 580 Å/min obtained in $CBrF_3$ at the same O_2 percentage. This clearly shows the lower Si removal efficiency of [Br] as compared to [F]. At higher levels of O_2, where the [F] level is depressed, the Si ERs in CF_4 and in $CBrF_3$ are very similar. The SiC etch rate is observed to increase nearly linearly with O_2 percentage up to 80% where it reaches the highest etch rate of ≈ 380 Å/min. Interestingly, this SiC etch pattern and ER levels are similar to those in CHF_3/O_2 plasma, where a H atom is found in place of the Br, and different from the pattern obtained in CF_4, where a F atom replaces the Br. In Si processing technology, $CBrF_3/CF_4$ mixtures are employed for the selective etching of poly-silicon over SiO_2, whereas CHF_3/CF_4 mixtures are utilized for the selective SiO_2 via etching. As shown in Fig. 5b, the etch rate cross-over point of SiC and Si occurs at $\approx 60\%$ O_2, and the highest SiC/Si ERR of ≈ 2 is observed at the usual high O_2 percentage (80 to 90%). The [F], [O], and [Br] plasma emission intensities are shown in Fig. 5c. The cross-over point between [F] and [O] occurs at $\approx 50\%$ O_2, which is approximately

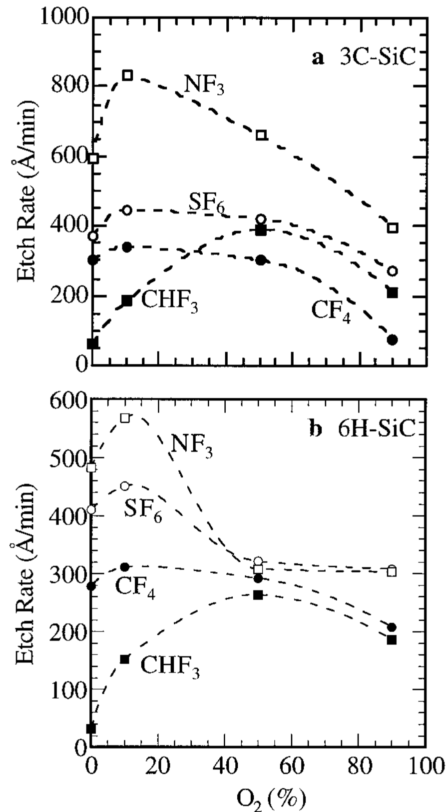

Fig. 6. Comparison of SiC etch rates in fluorinated/oxygen mixtures under the standard conditions for different polytypes. a) 3C-SiC, b) 6H-SiC

the same as for CHF_3/O_2 mixtures. It is interesting to point out that as the [F] level is relatively low and constant up to $\approx 50\%$ O_2, the linear increase in SiC etch rate with O_2 percentage in this range must be due to the increasing effect of C–O reactions.

4.1.6 Comparison of 3C- and 6H-SiC RIE

In general, as seen in Fig. 6, RIE of 3C-SiC grown on Si substrates results in a higher etch rate than that of 6H-SiC substrates. Based on current reported 3C-SiC material quality, a higher defect density of 3C-SiC heteroepitaxially grown on Si could in part enhance the charge transfer rate (chemical reaction). Unfortunately, there are no reports on the etching of 3C-SiC grown on 6H-SiC substrates. An indepth etching comparison between 3C-SiC grown on Si and 6H-SiC substrate is therefore difficult to make based on the limited current data.

4.1.7 3C-SiC effect of dc bias [53, 73]

The self-induced dc bias generated by plasmas using the fluorinated gases discussed above are shown in Fig. 7 as a function of O_2 percentage. Interestingly, the fluorinated gases which use more strongly electronegative species (e.g. NF_3 and SF_6) develop generally lower dc bias levels and higher etch rates than the other fluorinated oxygen plas-

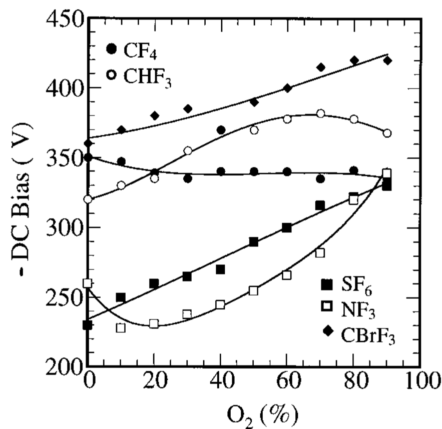

Fig. 7. The self-induced bias produced in the fluorinated plasmas of Fig. 1 to 5

mas. This would tend to indicate that the "cross-over" bias level separating the dc bias and reaction-rate limited SiC etching regimes [53] is a function of the etching gas used. The dc bias increases with O_2 percentage much more rapidly in NF_3/O_2 and SF_6/O_2, than for the other mixtures. In contrast, in CF_4/O_2 mixtures the self-induced bias remains nearly constant with O_2 percentage, while in CHF_3/O_2 and $CBrF_3/O_2$ mixtures the dc bias increases slowly as a function of O_2 percentage.

4.1.8 3C-SiC etching in remote NF_3/O_2 [79]

A remote plasma apparatus is frequently used for plasma-enhanced chemical vapor deposition (PECVD). In this case, a plasma produced remotely from the substrate is used to dissociate gas molecules in order to reduce the growth temperature. Pure NF_3 gas is currently used as a cleaning gas in PECVD to remove deposits from the reactor walls. The reason is the low polymer production of NF_3 plasma [80] and high etch rates of Si, SiO_2, and Si_3N_4 [81]. Interestingly, etching of 6H-SiC in a remote NF_3/O_2 mixture plasma hot-wall PECVD system has been reported with highly isotropic profile [79]. Although the etching experiment was performed at elevated temperature (330 °C), only a relatively low etch rate of 220 Å/min was obtained. In this case, thermal energy was the major energy input to the chemical etching process of SiC. The ion energy was limited by the plasma potential in which the sample was floating. This set of experimental conditions and results indicate that ion bombardment plays an important role in determining the SiC etching profile [53] and etch rate (through the breaking of the strong Si−C bonds). This confirms that both chemical and physical processes are needed in the etching of SiC which is in agreement with our previous discussion in Section 2 of this paper.

4.1.9 3C-SiC effect of crystallinity [72]

The effect of crystallinity on the SiC etch rate was explored by Padiyath et al. [72]. As shown in Fig. 8, they have found that etching of hydrogenated amorphous SiC (a-SiC), polycrystalline (poly-SiC), and crystalline 3C-SiC (c-SiC) in CF_4O_2 plasma at high dc bias (> 300 V) results in a decreasing etch rate with increasing level of crystallinity. This etch rate pattern is consistent with the trend in the number of broken Si−C bonds in

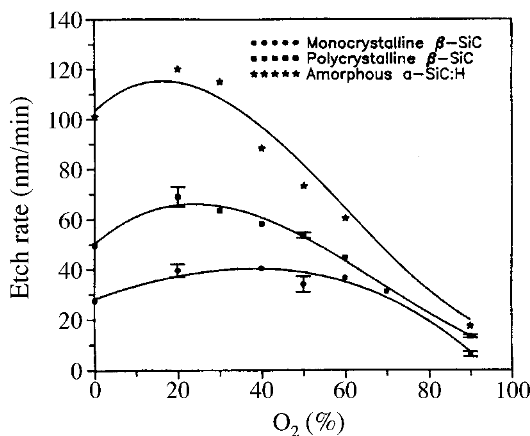

Fig. 8. Etch rates of 3C-SiC, poly-SiC, and a-SiC:H in CF_4 as a function of O_2 plasma [72]

these materials (c-SiC < poly-SiC < a-SiC), and hence the charge transfer rate during the chemical reaction process. The effect of crystallinity (or lack of it) on the etch rate is consistent with the effect of the dc bias, which increases the etch rate by partially damaging the SiC surface.

4.2 Mixtures of two fluorinated gases

In this section, we review the reactive ion etching of SiC in plasmas containing various combinations of two fluorinated gases. Since the fluorinated gases we have primarily investigated (CF_4, SF_6, NF_3, and CHF_3) each produce different etch rates, it was considered of general interest to investigate the effects of dual gas mixtures. The first set of mixtures consists of CHF_3 as the primary gas and CF_4, NF_3 and SF_6 as the secondary gases. Pure CHF_3 produces a residue-free etch surface but has a relatively low etch rate, while the reverse is the case for the other three gases. We were, therefore, interested in determining the residue-free parameter space obtainable with a dual fluorinated gas mixture. To that end, in this set of experiments data was obtained for the RIE of 3C- and 6H-SiC samples placed on the bare Al electrodes, which normally produces residues in the etch surface. The second set of experiments explored conditions for increasing the SiC etch rate while preventing residues through the use of a graphite cover on the Al electrodes. For these experiments, mixtures of NF_3 and SF_6 were used to etch 6H- and 4H-SiC samples.

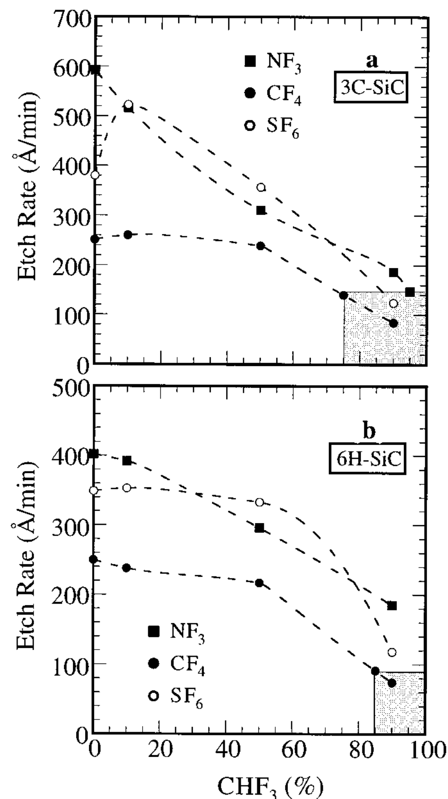

4.2.1 CHF_3 plus other fluorinated gases [82]

In this section we discuss the etching of SiC in dual fluorinated mixtures of CF_4/CHF_3, NF_3/CHF_3, and SF_6/CHF_3. As in the cases involving a mixture of a single fluorinated gas and oxygen (see Section 4.1), the experiments with dual fluorinated mixtures are performed with the standard etching conditions, and etch times of 5 and 30 min. Etch rates of 3C- and 6H-SiC in NF_3, CF_4, and SF_6 as a function of CHF_3 percentage are shown in Fig. 9a and b, respectively. The corresponding self-induced dc bias is shown in Fig. 10. The shadowed rectangular areas contain experimental conditions for which residue-free etching was obtained. A detailed

Fig. 9. Etch rates of a) 3C- and b) 6H-SiC in NF_3, CF_4, and SF_6 as a function of CHF_3 mixture plasmas. The shadowed rectangular area indicates a residue-free condition [82]

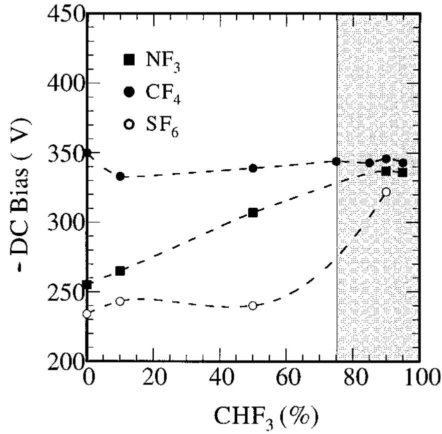

Fig. 10. Self-induced dc bias in fluorinated mixture plasmas [82]

discussion of the residue-free etching aspect is presented in the next section (Section 5) of this paper. Generally, 3C-SiC has a higher etch rate than 6H-SiC. In part, defect density in 3C-SiC [83] could be an important factor resulting in a higher etch rate. In Fig. 9, the experimental results (data points) were primarily obtained at 0, 10, 50, and 90% of CHF_3 in the total gas mixture. Additional data points were obtained for the residue-free etching study. Due to lack of full range of data points from 0 to 90%, dashed lines were used for the data point curve fitting for both Figs. 9 and Fig. 10. Without the O_2 additive effects, the [F] emission intensity changes almost linearly as a function of CHF_3.

Currently, etching of Si in fluorinated gas mixtures is frequently employed in the fabrication of Si integrated circuits. A variety of fluorinated gas mixtures, such as NF_3/CHF_3 [84], SF_6/CHF_3 [68], and CF_4/CHF_3 [66] have been reported for different applications. Usually, CHF_3 is used as a primary gas [66] for increasing selective etching of SiO_2 over Si, side-wall protection for anisotropic etching, resolving corrosion issues, and obtaining a residue-free (smooth) surface [68]. The CF_4/CHF_3 mixture has been particularly effective for the SiO_2 contact via and profile control etching. Under these near polymer formation conditions (without O_2 present in the main stream gas), care must be taken against contamination from particulate and excess polymerization. This could occur due to hydrogen-containing fluorinated gases (specially CHF_3) which produce more polymer than hydrogen-free gases (CF_4 and SF_6).

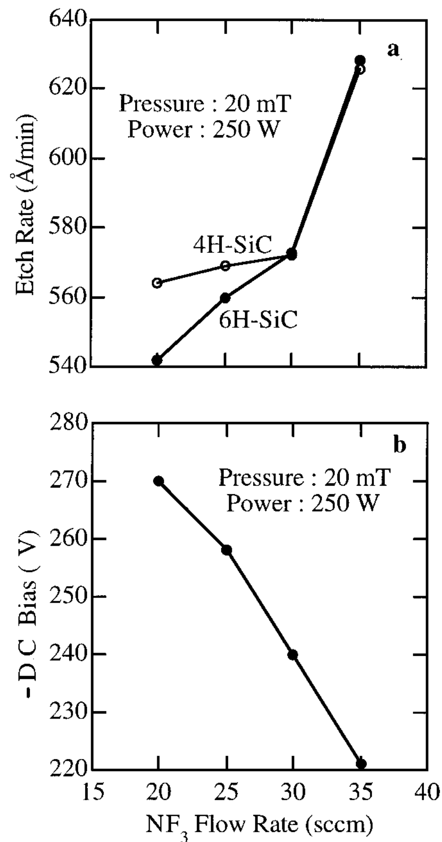

Fig. 11. Etch rate of 6H- and 4H-SiC vs. flow rate of NF_3

The etch rate of 3C-SiC generally decreases with increasing CHF_3 percentage in the dual gas mixtures. As shown in Fig. 9a, the most pronounced decrease occurs for the NF_3/CHF_3 and SF_6/CHF_3 mixtures. For example, the etch rate reduces from a high of 592 Å/min in pure NF_3 to 120 Å/min in the NF_3/90% CHF_3 mixture. In the case of CF_4/CHF_3 plasma, the etch rate was constant at low CHF_3 percentage, and much reduced compared to equivalent NF_3/CHF_3 and SF_6/CHF_3 mixtures. CF_4/CHF_3 mixtures containing more than 50% CHF_3 result in a reduction in etch rate similar to that of the other two mixtures.

The etch rates of 6H-SiC in the same dual fluorinated mixtures are shown in Fig. 9b. The highest etch rates for 6H-SiC were all obtained in pure NF_3, CF_4, and SF_6 gases and the etch rates in the dual mixtures generally decrease as the CHF_3 percentage increases. The etch rate of 6H-SiC in NF_3/CHF_3 mixtures decreases almost linearly with increasing CHF_3 percentage. Similar trends in etch rates were obtained for both of CF_4/CHF_3 and SF_6/CHF_3 mixtures.

Considering the dc bias and etch rate, it is interesting to note although both etch rates of 3C- and 6H-SiC fall in conditions of SF_6/50% CHF_3 > NF_3/50% CHF_3 > CF_4/50% CHF_3, the corresponding dc biases are in the reverse order of SF_6/50% CHF_3 < NF_3/50% CHF_3 < CF_4/50% CHF_3. This indicates a higher dc bias results in a lower etch rate, which means the etch rate does not have a simple linear relationship with the applied dc bias. However, a certain level of bias is required to physically or chemically etch SiC. To obtain a high etch rate, a combination of physical and chemical processes is generally required.

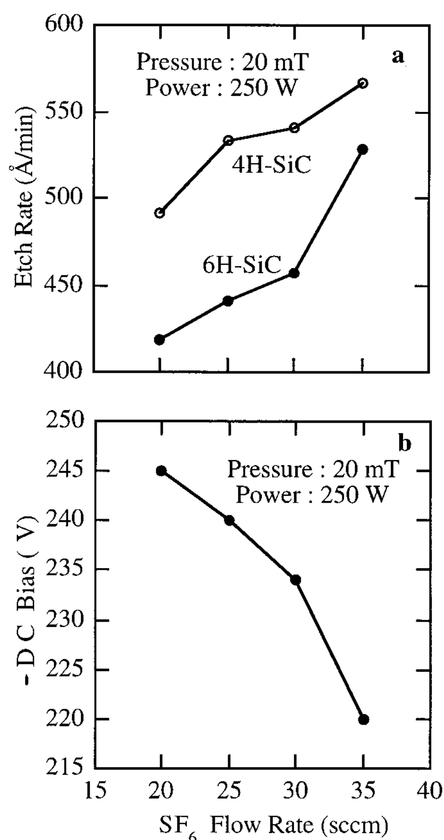

Fig. 12. Etch rate of 6H- and 4H-SiC vs. flow rate of SF_6

4.2.2 NF_3 plus SF_6 mixtures

4H- and 6H-SiC samples cut from single-crystal wafers were etched in mixtures of NF_3 and SF_6. The objective of investigating these dual fluorinated mixtures was to achieve higher etch rates, but without producing residues in the process. Therefore, we utilized a graphite cover between the Al electrode and the samples during RIE. Furthermore, we modified the standard etching parameters that was given in Section 3 (and followed in our previously reported results) by increasing the rf power from 200 to 250 W and investi-

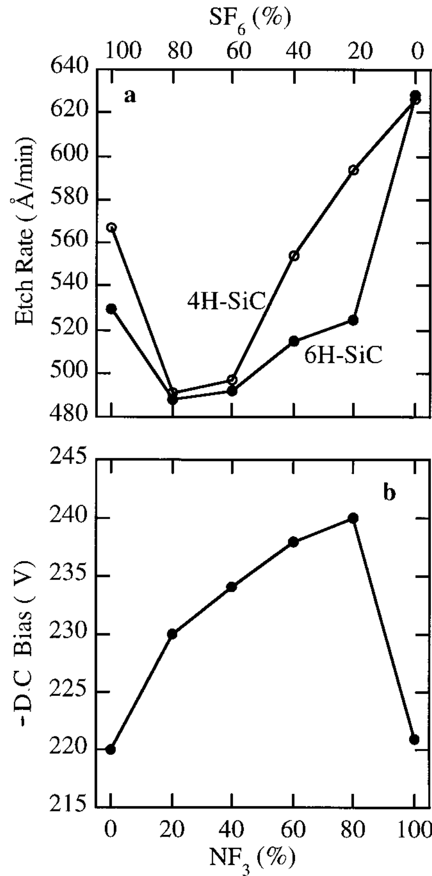

Fig. 13. Etch rate of 6H- and 4H-SiC in NF_3/SF_6 mixture plasmas

gating the effect of increasing the flow rate from 20 to 35 sccm (while keeping the pressure fixed at 20 mTorr). With these modifications, we found several conditions for which the resulting etch rate was greater than 500 Å/min, which is reasonably high for SiC RIE.

Figs. 11 and 12 show the etch rates of 4H- and 6H-SiC as a function of the flow rates of NF_3 and SF_6, respectively. The overall etch rate increases with the gas flow rate, despite the accompanying reduction in the residence time of the chemically active species. This shows that the critical flow rate is still not reached at 35 sccm. No significant difference in the etch rates for the two SiC polytypes was observed for NF_3, while for SF_6 the 4H polytype showed a somewhat higher etch rate (567 Å/min at 35 sccm) than the 6H polytype (529 Å/min at 35 sccm). The highest etch rate exceeded 600 Å/min in NF_3 plasma, and 500 Å/min in SF_6 plasma for both polytypes.

Fig. 13 shows the etch rates measured for the two SiC polytypes in different mixtures of NF_3 and SF_6 with a total flow rate of 35 sccm. The same general etch rate trend is

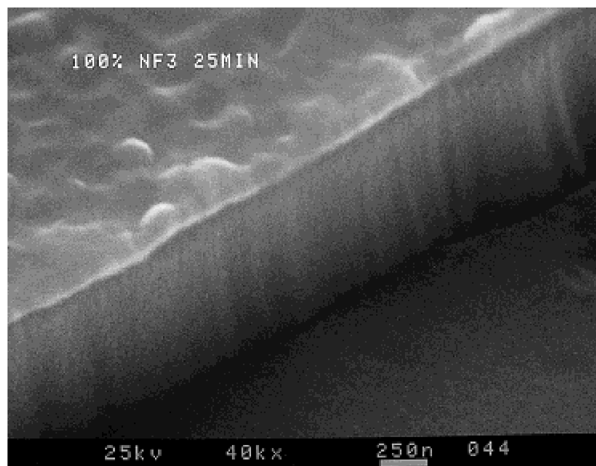

Fig. 14. SEM photograph of 6H-SiC (with 300 nm of Al mask) etched in pure NF_3 for 25 min under the following conditions: pressure: 20 mTorr, flow rate: 35 sccm, rf power: 250 W

Table 1
Summary of results reported on RIE of primarily hexagonal SiC polytypes

polytypes etched	source gas(es)	process type	typical process conditions: pressure, power, dc bias, flow rates	etch rate (Å/min)	ref.
3C	CF_4/O_2	plasma/ RIE (rf)	180 to 200 mT, 0.8 W/cm^2, 67% O_2, 33% CF_4	60 to 260	Dohmae et al. [85]
4H, 6H	SF_6	RIE (rf)	20 mT, 250 W, −220 to −250 V,		this work
			20 sccm	490, 420	
			35 sccm	570, 530	
6H	SF_6/O_2 NF_3/O_2	RIE (rf)	20 mT, 200 W, −220 to −250 V,		this work
			$SF_6 : O_2 = 18 : 2$ (sccm)	450	
			$NF_3 : O_2 = 18 : 2$ (sccm)	570	
6H	SF_6/O_2	RIE (rf)	50 mT, 200 W, −250 V, $SF_6 : O_2 = 5 : 5$ (sccm)	360	Kothandaraman et al. [86]
6H	SF_6/O_2, CF_4/O_2 with N_2 additive	RIE (rf)	190 mT, 300 W,		Wolf and Helbig [76]
			$CF_4 : O_2 : N_2 = 40 : 15 : 10$ (sccm)	2200	
			$SF_6 : O_2 : N_2 = 40 : 2 : 0$ (sccm)	3000	
4H, 6H	NF_3	RIE (rf)	20 mT, 250 W, −220 to −250 V,		this work
			20 sccm	565, 540	
			35 sccm	630	
4H, 6H	NF_3	RIE (rf)	225 mT, 275 W, −25 to −50 V, 95 to 110 sccm	1500	Casady et al. [78]
6H	$Cl_2/SiCl_4/O_2$ and Ar/N_2	RIE (rf)	190 mT, 300 W,		Niemann et al. [54]
			$Cl_2 : SiCl_4 : O_2 : N_2 = 40 : 20 : 8 : 10$ (sccm)	1600	
			$Cl_2 : SiCl_4 : O_2 : Ar = 40 : 20 : 0 : 10$ (sccm)	1900	
3C, 6H	SF_6/O_2	ECR (μwave)	1 mT, 1200 W, −20 to −110 V $SF_6 : O_2 = 4 : 0$ to 8 (sccm) $SF_6 : O_2 = 4 : 0$ to 6 (sccm)	1000 to 2700	Lanois et al. [87]
4H, 6H	CF_4/O_2	ECR (μwave)	1 mT, 650 W, −100 V, $CF_4 : O_2 = 41.5 : 8.5$ (sccm)	700	Flemish and Xie [88]

observed for both polytypes. A broad and shallow minimum in the etch rate occurs at 20 to 40% NF_3, while the highest etch rates are obtained for the pure gases. The fact that the etch rate of 4H-SiC is very close to that of 6H-SiC under most conditions enables us to transfer most RIE processes developed from one polytype to the other.

An example of RIE using pure NF_3 to etch a trench deeper than 1 μm is shown in Fig. 14. The etched surface and the sidewalls are quite smooth and without any residues (due to the use of the graphite cover). These process parameters could therefore provide favorable conditions for etching deep trenches in SiC for applications such as power device fabrication and micromachining.

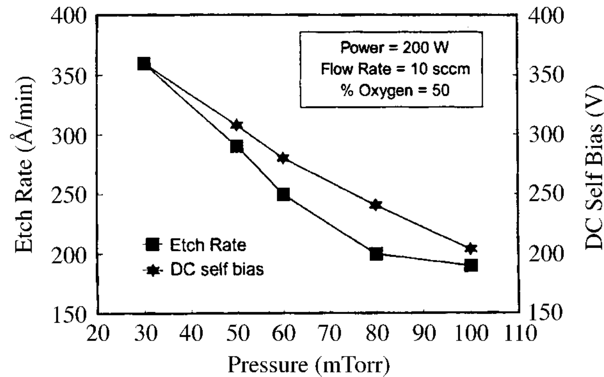

Fig. 15. Effect of variation in chamber pressure on etch rate and dc self bias [86]

4.3 Review of other results on SiC reactive ion etching

In this section, we review some of the results reported by other groups on primarily hexagonal SiC reactive ion etching. Table 1 summarizes the etching conditions and resulting characteristics. For completeness, selected results from our own work are also included. The table also contains information on microwave-based plasma etching of SiC, which is discussed in more detail in Section 6, and chlorinated gas plasmas, which is discussed in Section 5.3.2.

Plasma etching of different polytypes of SiC have been reported by other researchers. Dohmae et al. [85] reported the first plasma etching results on the 3C-SiC polytype. They used the CF_4/O_2 mixture at 180 to 200 mTorr to obtain plasma etch rate of 6 to 26 nm/min.

More recently, Kothandaraman et al. [86] have reported the effect of gas flow rate, chamber pressure, and rf power on the etch rate of 6H-SiC in SF_6/O_2 mixtures. Fig. 15

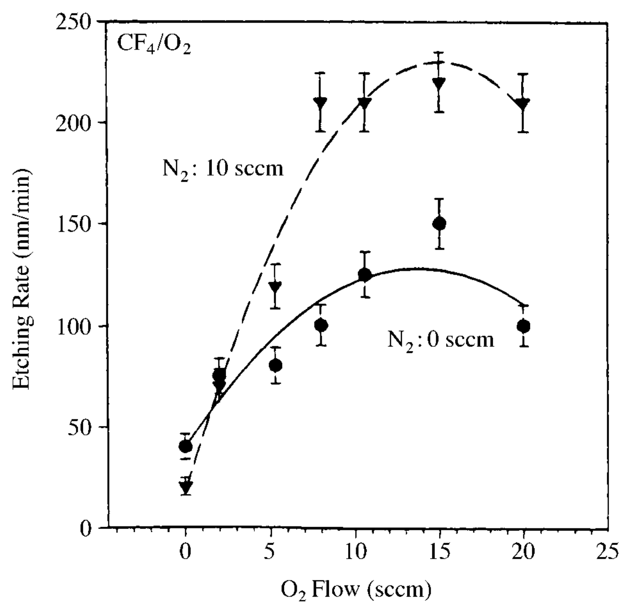

Fig. 16. RIE in CF_4 as a function of O_2 gas flow with and without N_2 additive [76]

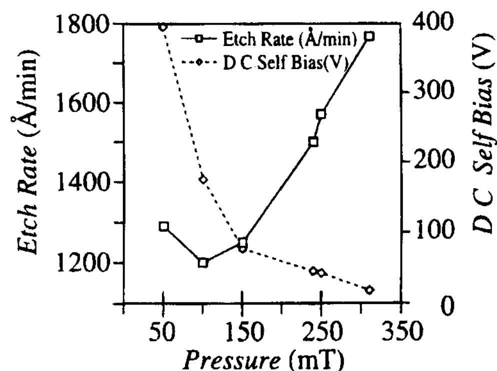

Fig. 17. Etch rate of 6H-SiC and self-induced dc bias as a function of chamber pressure with constant rf power of 275 W (1.7 W/cm^2) [78]

shows the variation of the etch rate as a function of pressure for a SF_6/50% O_2 mixture, an rf power of 200 W, and a total flow rate of 10 sccm. A peak etch rate of 360 Å/min was obtained at 30 mTorr pressure, which was the lowest pressure evaluated. Wolf and Helbig [76] have reported the effect of nitrogen additive to CF_4/O_2 and SF_6/O_2 plasmas on the etch rate of 6H-SiC at relatively higher pressure (190 mTorr). As seen in Fig. 16, the etch rate at this pressure is enhanced by a factor of 1.5 to 2 through the addition of N_2 in CF_4/O_2 plasmas. In SF_6/O_2, the etch rate is higher than for CF_4/O_2 and actually decreases with N_2 addition due to the formation of complex molecules. Casady et al. [78] have reported RIE of both 6H- and 4H-SiC polytypes in pure NF_3 source gas at a very high flow rate of 100 sccm. As shown in Fig. 17, the etch rates obtained exceed 1200 Å/min, and increase almost monotonically as the pressure is increased from 75 to 325 mTorr. They report an optimum pressure of $\approx$225 mTorr for best etch rate and surface cleanliness.

5. Techniques for Obtaining Residue-Free Etching

Interestingly, SiC etching in most of the fluorinated oxygen plasmas results in residue formation (surface roughness) [89] in the etch field except in some of the CHF_3 plasma conditions for all SiC polytypes [73, 75]. It has been shown using Auger surface analysis [67, 89] that residues were formed due to contamination from the cathode material through the micromasking effect. Several issues need to be addressed regarding how the residues are formed. As discussed before, the electrode area in the commercially available RIE systems is much larger than that of the SiC samples utilized in the etching experiments. This results in simultaneous etching (sputtering) of the metal electrode, leading to residue formation. Residue-free etching of SiC using graphite or kapton sheet to cover the Al elecrode has reaffirmed the micromasking effect [67, 73, 75].

To obtain residue-free etching of SiC, we have previously reported the use of fluorinated oxygen mixtures such as CHF_3/O_2, CF_4/O_2, SF_6/O_2, and NF_3/O_2 with H_2 additive [73, 75], and of mixtures of two fluorinated gases such as CF_4/CHF_3 and NF_3/CHF_3 [82]. In this paper, we review several approaches to prevent residue formation in the etch field including (i) adding pure H_2 gas into fluorinated oxygen plasmas; (ii) utilizing H-containing gas as one of the etching gases, such as CHF_3; (iii) employing high density plasma sources – sample bias control and control of the location of the sample which is separated from plasma generation region; (iv) covering the metal exposed to the plasma by using teflon, graphite, and kapton. The trade-off between residue formation and other etching parameters is presented.

We have previously demonstrated the etch rate and anisotropic profile of SiC in a variety of fluorinated oxygen and fluorinated mixture plasmas, such as CHF_3/O_3, $CBrF_3/O_2$, CF_4/O_2, SF_6/O_2, NF_3/O_2, CF_4/CHF_3, SF_6/CHF_3, and NF_3/CHF_3. Considering the surface morphology after long term etching, rough surfaces (residues) were obtained after etching in most of these gas mixtures. The density and physical shape of residues were determined by the plasma chemistry [73, 75]. Interestingly, similar rough surfaces were reported for Si etching in pure CF_4 plasma [90, 91]. The mechanism proposed was again metal contamination from the electrode. The rough etched surface usually shows as black when observed directly under room light. This is due to the scattering of light from the surface microstructure. These areas have been called "black silicon". For n-type 6H-SiC, we observe dark non-transparent green areas with residues in the etch field. To remove the electrode metal contamination, H_2 additive in pure CF_4 plasma has been reported in Si RIE etching [90]. H_2 could possibly be seen as an aluminum scavenger ("gettering effect"). This indicates that the H_2 additive process could not only be applied to just Si and SiC, but possibly to any semiconductor material in general [92]. In addition to using H_2 to obtain a residue-free etched surface, it has been used as an additive in fluorinated plasmas for the selective etching of SiO_2 and Si_3N_4 over Si [66]. One of the side effects of the H_2 additive in the plasma is that the H radicals are implanted into the Si substrate, and deactivate the dopants [93, 94]. Implant depths of 400 Å into the Si substrate were reported [95] resulting in the possible reduction of the surface doping concentration. This result has been confirmed [56] by fabricating Schottky diode to measure the surface doping concentration under various etching conditions.

To obtain a residue-free etching of 3C- and 6H-SiC, one can (i) etch in fluorinated oxygen mixture with H_2 additive, such as $CHF_3/O_2/H_2$, $CF_4/O_2/H_2$, $SF_6/O_2/H_2$, and $NF_3/O_2/H_2$ [73, 75]; (ii) etch in CF_4/CHF_3 and NF_3/CHF_3 fluorinated mixtures [84]; (iii) perform etching with the electrode covered with a non-metallic sheet [67, 73, 75]. These processes for residue-free etching can easily be utilized by choosing the right etchants or by covering the electrode with graphite, polymide, or quartz sheet. Possible mechanisms have been proposed including (i) gettering effect − gas phase reaction of H_2 and Al clusters to form aluminum hydride volatile compounds (AlH_x); and (ii) etching enhancement of carbon-rich surface. A material with low etch rate and sputter yield could be the best candidate. Care must be taken to avoid excess polymerization or particle generation in this case. The greatest advantage of using H_2 additive for residue-free etching is that the process is independent of the reactor material, and is highly reproducible and portable. However, H_2 addition also results in a reduction of the etch rate due to gas phase reaction of fluorine and hydrogen. The presence of excess H_2 in the plasma also reduces the etch aspect ratio. This is because the hydrogen-containing fluorinated gases produce more polymer than hydrogen-free gases [66]. A trade-off between residue-free etching with H_2 process and other etching requirement is often needed.

5.1 H_4 additive in fluorinated oxygen mixtures

5.1.1 Etching of 3C-SiC [73]

Etching of 3C-SiC in fluorinated oxygen mixture plasmas has been reviewed in detail in the previous section. Adding pure H_2 in the fluorinated oxygen plasmas can prevent residue formation. Due to the gas phase reaction between fluorine and hydrogen, various levels of H_2 are required under a variety of etching conditions. The 3C-SiC etch rate in

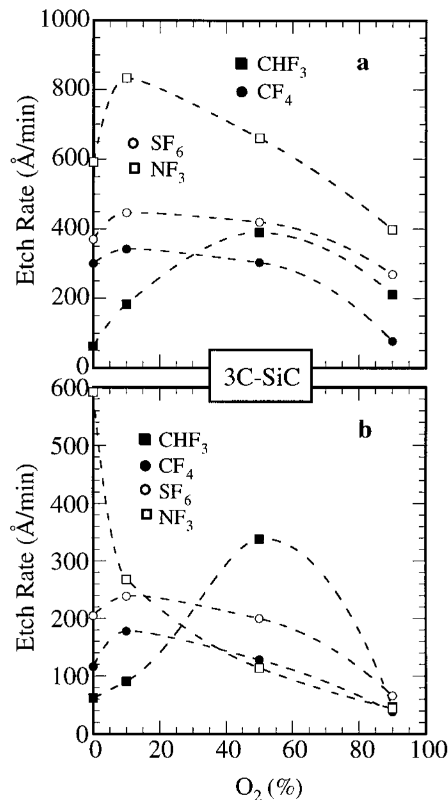

Fig. 18. Etch rates of 3C-SiC a) without and b) with H_2 additive in CHF_3, CF_4, SF_6 and NF_3 as a function of O_2 plasma [73]

CHF_3, CF_4, SF_6, and NF_3 as a function of O_2 plasma without and with H_2 additive is shown in Fig. 18a and b, respectively. The corresponding minimum H_2 flow rate of Fig. 18b is shown in Fig. 19. As shown in Fig. 18, limited data points were measured at 0, 10, 50, and 90% of O_2 so that the dashed line was employed for the curve fitting. Generally, the etch rate decreases as the H_2 percentage increases. This is the reason why finding the minimum H_2 flow rate is so important. Furthermore, the minimum H_2 flow rate required for residue-free etching in fluorinated oxygen gas mixtures decreases as the O_2 percentage in the mixture increases. This is due to increased consumption as a result of the gas phase reaction. An exception is the CHF_3/O_2 plasma. This may be because CHF_3 is by itself a H_2-containing gas. Etching in pure NF_3 plasma with few spikes was obtained only for 3C-SiC with high etch rate and anisotropic profile. As shown in Fig. 19, 16 sccm H_2 was used as the highest flow rate in all of the fluorinated oxygen mixture plasmas we have investigated. As the required H_2 flow rate is greater than 16 sccm, no further experiments were performed to find the minimum H_2 flow rate. As shown in Fig. 18b, the highest residue-free etch rate of $\approx$338 Å/min was obtained in CHF_3/50% O_2 (20 sccm) with H_2 (2 sccm) additive plasma. The process pressure was changed from 20 to 25 mTorr.

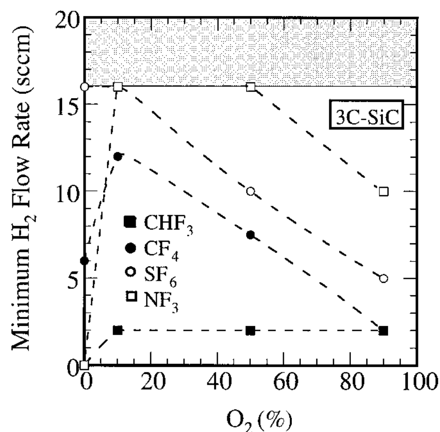

Fig. 19. Minimum H_2 flow rate of residue-free etching condition for 6H-SiC in fluorinated oxygen plasmas [73]

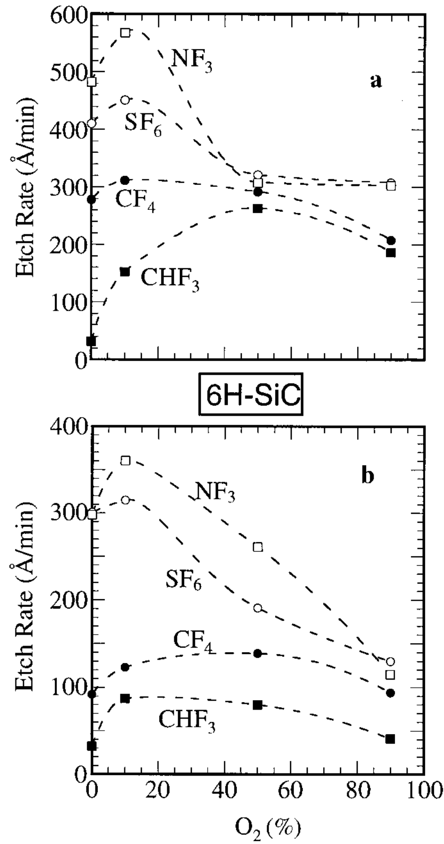

Fig. 20. Etch rates of 6H-SiC in CHF_3/50% O_2 a) without and b) with H_2 additive in CHF_3, CF_4, SF_6 and NF_3 as a function of O_2 plasma [73]

5.1.2 Etching of 6H-SiC [75]

Etching of 6H-SiC in CHF_3, CF_4, SF_6 and NF_3 as a function of O_2 plasma without and with H_2 additive is shown in Fig. 20a and b, respectively. The corresponding H_2 flow rate of Fig. 20b is shown in Fig. 21. As shown in Fig. 20, limited data points were measured at 0, 10, 50, and 90% of O_2 so that the dashed line was employed for curve fitting. As for 3C-SiC, the etch rate generally decreases as the H_2 percentage increases. The highest etch rates were obtained by using the minimum H_2 flow rate needed for residue-free etching. As shown in the shadowed rectangular region of Fig. 21, an upper limit of 16 sccm was set for the H_2 flow rate. As shown in Fig. 21, for the NF_3/O_2 and SF_6/O_2 mixtures, residue-free etching condition was obtained only at 90% O_2 for both mixtures. The etch rate obtained was ≈150 Å/min. At low O_2 percentage, the minimum H_2 requirement for residue-free etching increases significantly. Except for the CF_4/10% O_2 composition, residue-free etching was obtained in both CF_4/O_2 and CHF_3/O_2 mixtures with <16 sccm of H_2 additive. Comparing the H_2 requirement to 3C-SiC (Fig. 19), 6H-SiC needs a higher level of H_2 to prevent the residue formation. The reason is still unknown based on the current

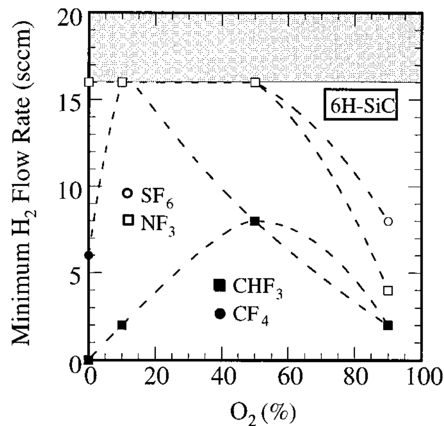

Fig. 21. Minimum H_2 flow rate of residue-free etching condition for 3C-SiC in fluorinated oxygen plasmas [73]

experimental results. As shown in Fig. 20b, the highest residue-free etch rate of ≈150 Å/min was obtained in CF_4/50% O_2 + H_2 (28%) mixture plasma. The process pressure was changed from 20 to 30 mTorr.

5.2 Fluorinated mixtures

CHF_3 is the only fluorinated plasma in which residue-free etching can be obtained for both 3C- and 6H-SiC polytypes without any gas additive and without the need for covering the Al electrode. Unfortunately, the etch rate in pure CHF_3 plasma is much lower compared to the etch rates in the plasmas of other fluorinated gases investigated i.e. NF_3, CF_4, and SF_6. Hence the mixtures of these gases with CHF_3 as the primary gas have been employed for the etching of 3C- and 6H-SiC to get a higher etch rate while maintaining residue-free etching. The etch rate and etched surface morphology of 3C- and 6H-SiC in NF_3, CH_4, and SF_6 as a function of the percentage of CHF_3 in the mixture are shown in Fig. 9a and b, respectively [82]. The corresponding dc bias is shown in Fig. 10. Etch rate in fluorinated mixture plasmas has been discussed previously (Section 4.2) and elsewhere [82]. Residue-free etching of 3C- and 6H-SiC in fluorinated mixture plasmas has been obtained in the shadowed rectangular region of Fig. 9. As shown in Fig. 9a, residue-free etching of 3C-SiC was obtained only in CF_4/CHF_3 and NF_3/CHF_3 mixture plasmas. At CHF_3 percentages higher than 75%, residue-free etching can be obtained in CF_4/CHF_3 mixtures. In this paper, we have expressed this as CF_4/ >75% CHF_3. With this nomenclature, NF_3/ >95% CHF_3 is required to obtain residue-free etching for the 3C-SiC. In addition, even though the mixture of SF_6/90% CHF_3 is located in the residue-free etching region in terms of etch rate, no residue-free etching was found in the mixture of SF_6/CHF_3.

For 6H-SiC, as shown in Fig. 9b, CF_4/CHF_3 is the only fluorinated mixture plasma in which we can achieve residue-free etching. CF_4/ >85% CHF_3 is required for this condition. Comparing to 3C-SiC (Fig. 9a), etching of 6H-SiC (Fig. 9b) needs a higher level of CHF_3 to achieve residue-free conditions. Interestingly, this result is similar to that for the H_2 additive in fluorinated oxygen mixture plasmas i.e. a higher level of H_2 is needed for 6H-SiC to obtain residue-free etching. In NF_3/CHF_3 plasma, even at NF_3/ >95% CHF_3, residues in the etch field were obtained in 6H-SiC, whereas residue-free etching was obtained in 3C-SiC for these compositions. This difference in the etch results for

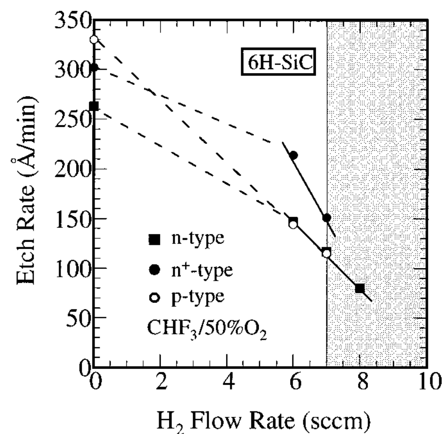

Fig. 22. Etch rate 6H-SiC of various doping in CHF_3/50% O_2 as a function of H_2 flow rate [75]

3C- and 6H-SiC for the same gas composition can be used to identify the polytype by employing RIE. Similar to 3C-SiC, residue-free etching could not be obtained in SF_6/CHF_3 mixtures for 6H-SiC as well.

To study the residue-free etching process on various doping levels and dopant type, n-, n^+-, and p-type 6H-SiC samples were etched in CHF_3/50% O_2, and the minimum hydrogen additive required for each was evaluated. The doping level of n-, n^+-, and p-type 6H-SiC are about 10^{17}, 10^{19}, and 10^{18} cm^{-3}, respectively. The etch rate with different doping level and dopant types as a function of H_2 flow rate are shown in Fig. 22. Similar etch rates were obtained for the n- and p-type samples. The n^+-type 6H-SiC samples, however, had a somewhat higher etch rate. Similar levels of H_2 (7 to 8 sccm) were required to obtain residue-free etching for samples with different doping level and dopant type. This result indicates that the doping level and the dopant type is insignificant for the residue-free etching process utilizing H_2 additive.

5.3 Other techniques for residue-free etching

5.3.1 Non-metallic electrodes

Metal contamination (micromasking) from the electrode or surrounding reactor wall is the main source for contamination resulting in residues in the etch field. The easy way is to cover with non-metallic material such as SiO_2, Si, graphite, kapton, and teflon. A low etch rate and sputter yield material can be the best candidate. Notably, loading effect from the covering material becomes inevitable during etching. In Si technology, the most common material used to cover the electrode/reactor walls is teflon. Since most systems are designed for etching Si wafers, teflon could be used to cover the entire metal surface so that one can easily minimize the metal contamination during the etching process. However, for SiC, we have reported [73, 75] that it is sufficient to cover the powered electrode (sample electrode) by a graphite or a kapton sheet and that we can leave the upper electrode and the reactor walls intact (without covering). Since the material is in form of a thin sheet, it does not affect the distance between the electrodes. One should be aware that the use of a covering material could change the discharge conditions by leading to polymer formation (if the cover material is a polymer), and by altering the distance between the electrodes (if the sheet is too thick). However, utilizing the right material for the etch mask, and avoiding metal contamination from the etching reactor can prevent the formation of residues in the etch field.

5.3.2 Non-fluorinated plasmas

RIE of 6H-SiC in chlorine-based plasmas (Cl_2/$SiCl_4$/O_2/Ar/N_2) has been reported by Niemann et al. [54]. Interestingly, non-metallic CVD SiO_2 was employed as the etch mask and the SiC sample was affixed on the oxidized Si wafer to facilitate the transferring system. Although the size (1″) of SiC wafer is small, the Si wafer can fully avoid the contamination from the metallic electrode. No residues were observed in this gas mixture. A higher etch rate of (1 to 2) $\times 10^3$ Å/min was obtained in this gas mixture by varying the flow of O_2 and choosing Ar or N_2 inert gas independently. These experiments show promising results for SiC etching in Cl-based plasma with a high etch rate and non-metallic etch mask. However, higher processing costs usually accompany the use of chlorinated plasma-assisted etching. Further investigation of SiC etching in chlorine based plasmas are required to compare the etch rate and etched surface morphology to those obtained in fluorinated plasmas.

6. Etching in High Density Plasmas

As we progress into the Si Ultra-Large-Scale Integrated (ULSI) circuit era, Si technology is currently employing etching at lower pressures (< 10 mTorr) and use of higher density (10^{10} to 10^{12} cm^{-3}) plasmas. Such plasmas have relatively lower plasma potential and higher ionization efficiencies [66], and it is possible to have independent control over the ion energy and the flux to the wafer. They are able to provide sufficient plasma densities for etching feature sizes below 1 μm and for aspect ratios (depth/width) much larger than one. Etching in such plasmas results in a higher etch rate (and thus a higher throughput) and a highly anisotropic etch profile (desirable for sub-μm etching). The process utilizes lower pressures which reduces the scattering of ions and increases directionality, thus giving more control over the etch profile and a better etch uniformity. This is extremely important when device size shrinks to < 1 μm. The process also results in reduced surface damage (and hence lower leakage current), and allows the use of pure etchant gases without the need for additives to avoid residues. These advantages make it desirable to perform dry etching of SiC in high density plasmas. With etch rates higher than 1000 Å/min, reactors utilizing such plasmas would be able to fulfill the nominal mass-production requirement at a throughput of ≈10 wafers/h when larger area SiC wafers would be used for device fabrication. Investigation of etching of SiC in high density plasmas could indeed be an active area for research.

Many widely used high density plasma systems employ electron cyclotron resonance (ECR), and in such systems, the samples to be etched are placed remotely from the plasma generation region. Recently, plasma etching of 6H-SiC has been reported [55] in ≈CF_4/20% O_2 plasmas with relatively lower dc bias (< 200 V). A higher etch rate and a residue-free ("smooth") surface was obtained without any gas additive. The absence of residues in this process indicates that there is negligible sputtering from the etch mask and the electrode materials. Interestingly, indium tin oxide (ITO) has been employed as an etch mask material rather than aluminum (Al). Although a higher etch rate was obtained in ECR etching, a higher input power (> 500 W) was utilized to achieve this goal. The results reported from ECR etching in CF_4/O_2 plasma [55] are shown in Fig. 23. To understand the advantages of SiC ECR etching over RIE, it is important to consider the discharge mechanism and conditions of the ECR plasma. ECR plasma can

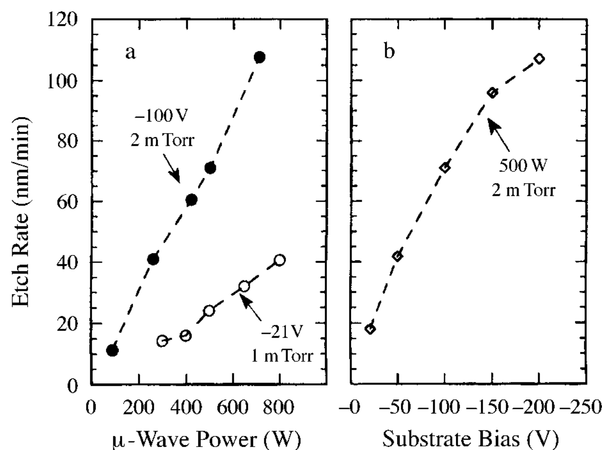

Fig. 23. Etch rates of 6H-SiC in ≈CF_4/20% O_2 ECR plasma as a function of a) input μwave power and b) applied rf bias power [55]

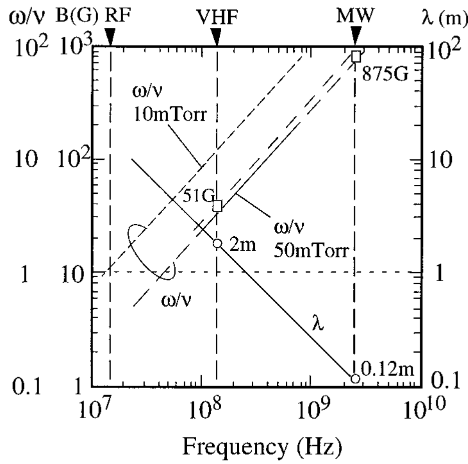

Fig. 24. Conditions of electron cyclotron resonance (ECR) plasma as a function of frequency [92]

be produced either by microwaves (μwave) or by VHF waves with different levels of magnetic flux density [96]. ECR plasma parameters such as excitation frequency and magnetic field as a function of frequency are shown in Fig. 24. The condition of $\omega/\nu \gg 1$ should be satisfied, where $\omega(2\pi f)$ and ν are the angular frequency and electron collision frequency, respectively. The magnetic field corresponding to μwave and VHF waves are 875 and 51 G, respectively. The value of ω/ν also indicates the intensity of the plasma. Under certain pressure (<5 mTorr), a plasma density higher than that in RIE can be obtained from charge particle resonance.

In addition to ECR plasmas, there are many other high density remote plasma sources commercially available, such as the Transformer/Inductive Coupled Plasma (TCP/ICP) [97], Helicon (H) Plasma [98 to 101], and the Helical Resonance (HR) Plasma [102, 103]. For comparison, the plasma density of various plasma sources as a function of pressure is shown in Fig. 25. The plasma density decreases as the pressure increases. Generally, the RIE plasma density is in the range of 10^9 to 10^{11} cm^{-3}. The plasma density in an RIE reactor can be enhanced by confining the charge particles with a magnetic field. This process is referred to as magnetically enhanced reactive ion etching (MERIE). However, in the presence of the magnetic field, plasma uniformity in such a process becomes a key issue. To have a generic idea of the various plasma sources, system schematic diagrams of RIE, PE, ECR, TCP/ICP, H, and HR plasma are shown in Fig. 26. RIE (Fig. 26a) and PE (Fig. 26b) are both capacitively coupled

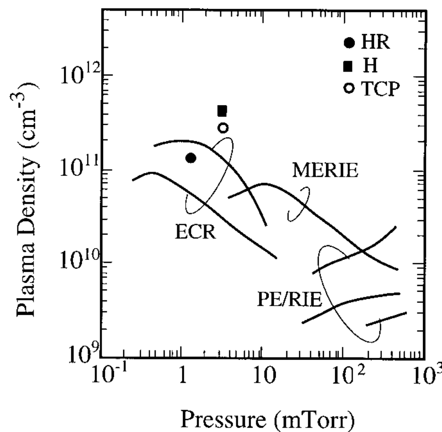

Fig. 25. Plasma densities as a function of pressure in various plasma sources

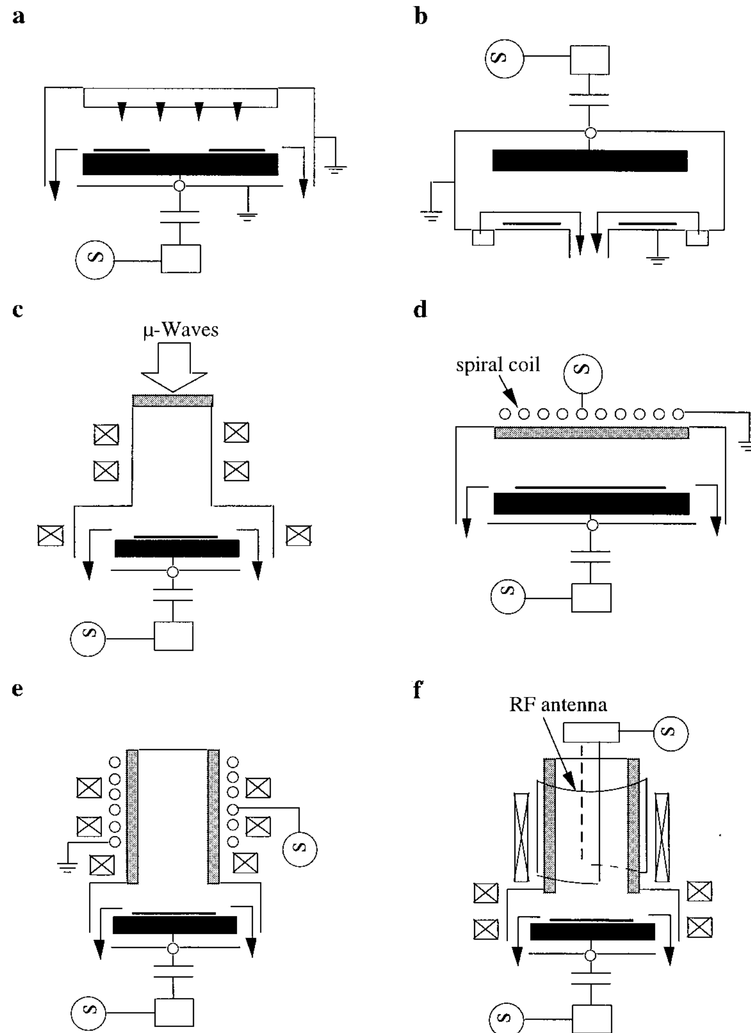

Fig. 26. System configuration of remote plasma sources: a) reactive ion etching (RIE), b) plasma etching (PE), c) electron cyclotron resonance plasma (ECR), d) transformer coupled plasma (TCP), e) helical resonance plasma (HR), f) helicon plasma (H)

plasmas (low plasma density and high plasma potential). For RIE, the area of the bottom electrode (wafer electrode) is smaller than that of upper electrode so that a higher sheath bias can be generated across the wafer. The wafer to be etched is placed on the electrode that has the higher bias and hence ion bombardment can participate in the overall etching process.

The discharge mechanisms of TCP/ICP [104], H [105, 106], and HR [107] plasma have been reported elsewhere. A detailed discussion on these plasmas is beyond the scope of this paper. However, a brief discussion is given next. The transformer coupled plasma (Fig. 26d) is generated by the application of rf power to a non-resonant, induc-

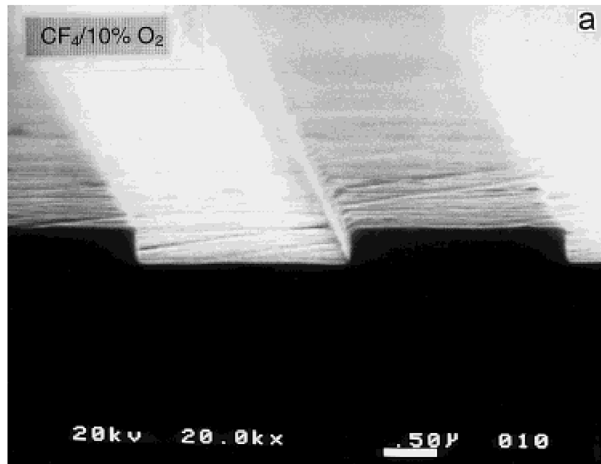

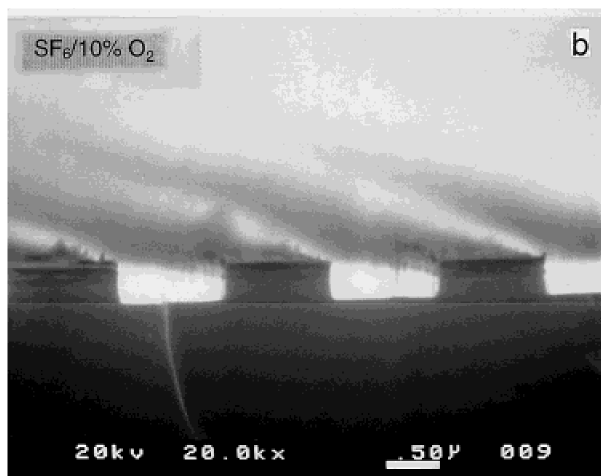

Fig. 27. Helicon plasma etching of 6H-SiC at 10 mTorr in a) CF_4/10% O_2 and b) SF_6/10% O_2

tive coil, resulting in the breakdown of the process gas within or near the coil by the induced rf electric field. Power is mainly transferred from the electric field to the plasma electrons by collision dissipation (ohmic heating). Inductive sources have several advantages over other sources, including simplicity in concept, no need for magnetic field (resulting in better plasma uniformity), non-resonant operation, and cable-ready rf power (no waveguide needed). The helical resonator plasma (Fig. 26e) is created by either capacitive or inductive coupling. Careful hardware design can force the operation in the desired inductive mode (high density and low plasma potential). Helicon plasma (Fig. 26f) is excited by an rf-driven antenna that is coupled with the transverse mode structure across an insulating chamber wall. The input energy is absorbed by the electrons in the plasma through collision or through Landau damping.[2]) Currently, high

[2]) Landau damping is a process by which a wave transfers energy to electron having velocity near the phase velocity $\nu_{ph} = \omega/k_z$ of the wave.

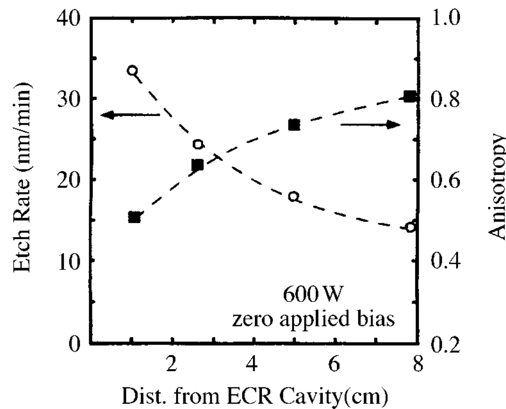

Fig. 28. Effect of sample proximity in ECR system on SiC etch rate and anisotropy of etching [88]

density plasma sources are being widely utilized in the fabrication of Si ULSI circuits [108 to 111].

We have explored the etching of SiC in the helicon plasma. In these experiments, we performed the etching of n-type 6H-SiC substrate in $CF_4/10\%\ O_2$ and $SF_6/10\%\ O_2$ gas mixtures with an input rf power (helicon source) of 1000 W, an applied rf bias power of 100 W, a process pressure of 10 mTorr, and a total gas flow rate of 44 sccm. Al was employed as the etch mask. Using kapton tape, the SiC sample was affixed to a large area glass substrate (Corning 7049) to facilitate the automatic transferring system into the etching reactor. The sample is located right underneath the plasma generation zone and the area is much smaller than the glass plate. We can assume that there was no metal contamination from the electrode which was covered by the glass plate. Under this condition, the only possible contamination source is the etch mask. The etching profiles with etch mask in place in $CF_4/10\%\ O_2$ and $SF_6/10\%\ O_2$ plasmas are shown in Fig. 27a and b, respectively. As shown in Fig. 27, highly anisotropic etching profiles were obtained from both mixture gases. The result obtained in SF_6/O_2 reaffirmed that SiC does enhance the polymer formation during etching to prevent the side wall from being etched (no undercut). In these experiments, the etched area was ≈10% of the

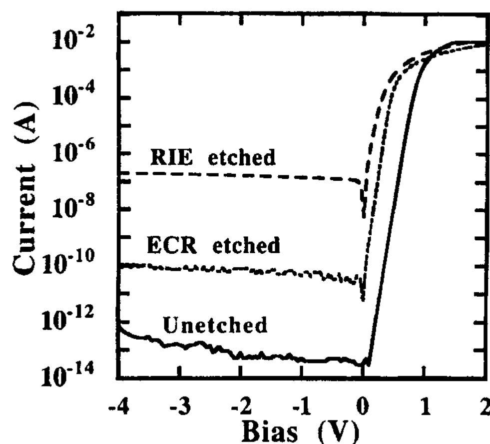

Fig. 29. Current–voltage characteristics of Pd Schottky diodes on RIE etched with addition of H_2, ECR etched, and unetched SiC samples [56]

total sample electrode area exposed to the plasma. The plasma was generated inside a quartz tube and the SiC sample was located on top of the glass plate. Interestingly, residues were found fully covering the etch field in both mixture gases. This is in contrast to ECR plasma etching in which no residues were reported. The possible explanation for residues in the etch field is etch mask contamination. These results indicate that etching in high density plasma does not always result in residue-free etching. Optimization of process conditions including etch mask material, etching condition, and system configuration is required to achieve a high etch rate and residue-free etching.

ECR plasma etching using microwave plasma has been reported by Lanois et al. [87] and Flemish and Xie [88]. Lanois et al. achieved an etch rate of 100 to 270 nm/min for both 3C and 6H polytypes. Flemish and Xie reported effective control of the etch profile and morphology of 4H- and 6H-SiC polytypes using CF_4/O_2 mixtures. Fig. 28 shows the effect of sample proximity to the ECR source on the etch rate and anisotropy. The anisotropy can be quantified as $A = (d - l)/d$, where d and l are the vertical and lateral etch depths, respectively. In addition, ECR etching has been reported [56] to produce significantly reduced damage on the SiC surface. Fig. 29 shows the current–voltage characteristics of Pd Schottky diodes formed on the unetched SiC surface, as well as on RIE etched and ECR etched surfaces. The ECR etched surface results in a much reduced leakage current compared with the RIE etched case.

7. Etching of Sub-μm Features

Sub-μm reactive ion etching is one of the critical processes for device fabrication when the device size shrinks to < 1 μm. In the etching of Si sub-μm features, highly anisotropic etching profile is necessary. Microloading and microscopic etching uniformity are the two key issues for the etching of sub-μm features [112]. Microloading effect is dependent on the microstructure density in the etched area and the gas depletion near the surface. Microscopic etching uniformity refers to achieving similar etch depths and profiles throughout the surface of the wafer. Due to reasons such as gas depletion and plasma non-uniformity, a wide open etched area often exhibits a higher etch rate than that observed in the smaller areas (microloading). Ion scattering results in an unexpected etching profile depending on the process pressure and the etchant gas. For SiC, basic digital integrated circuit on a single wafer is still under development [113]. Applying the same principles as for Si, a high degree of etching profile control is required for the etching of sub-μm SiC. To achieve this condition, gases resulting in higher etch rates such as NF_3 and SF_6 are advantageous. For example, we have previously reported [73] etching of 3C-SiC in pure NF_3 and $NF_3/10\%\ O_2$ mixture with etch rates in excess of 600 Å/min, and a highly anisotropic profile ratio (vertical-to-lateral etch distance) of 10:1 to 15:1 (equivalent to $A = 0.9$ to 0.93). It is important also to consider the issue of etch residues during sub-μm etching under these conditions because metal contact is usually the subsequent process.

8. Etching Conditions and Trade-Offs

In the previous sections, RIE etching of SiC has been shown to produce usable etch rates (100 to 1000 Å/min) and a high degree of etching anisotropy [53, 73, 75]. In most cases, the etch rate increases proportionately with the input rf power [53]. To obtain

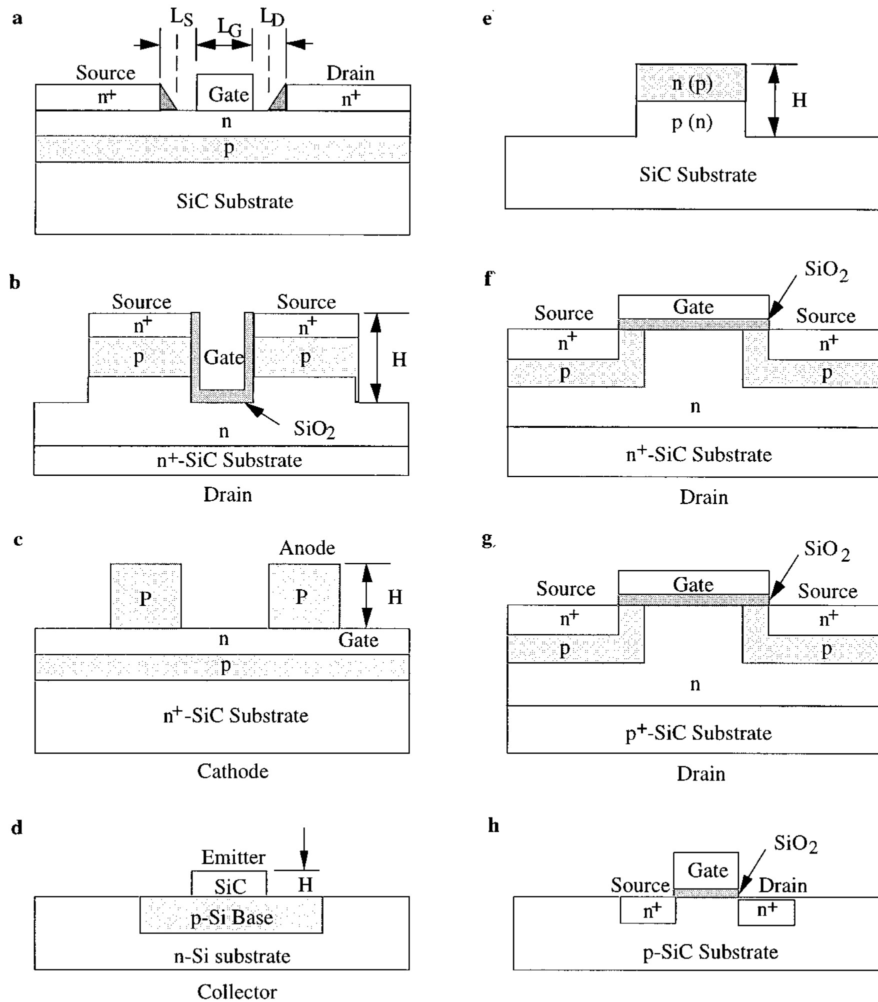

Fig. 30. Device structures: a) MESFET, b) UMOS, c) thyristor, d) HBT, e) diode, f) DMOS, g) IGT, and h) MOS [111]. H indicates the etch step height

residue-free etching of SiC, one can utilize either H_2 additive in fluorinated oxygen gas mixtures or H_2 containing gas in fluorinated gas mixtures. Both these approaches suffer from a reduced etch rate and anisotropy. For example, in the fluorinated mixture, one could obtain an etch rate of only ≈ 150 Å/min and an etch aspect ratio (depth/width) of ≈ 3 to 4, equivalent to anisotropy $A = 0.66$ to 0.75. From a device fabrication point of view, higher etch rates and etch aspect ratios are desirable for etching of trenches for power devices and for device isolation. For example, as shown in the cross-sectional view of a MESFET in Fig. 30a, the surface morphology of gate trench etching becomes extremely important for the subsequent gate metal deposition. In a currently published MESFET device structure [14], a 0.15 μm n^+ SiC layer has been used for forming the metal–semiconductor contact. The length of the gate (L_G), and spacing gate–source (L_S) and

Table 2
Summary of etching results and issues on RIE of 3C-SiC

issues	source gas(es)	≈ etch rate (Å/min)	selectivity SiC/Si	etch aspect ratio	residue-free[a])
high selectivity	CHF_3/80% O_2	350	2		N
	$CBrF_3$/80% O_2	380[b])	2		N
	CF_4/80% O_2	200	2		N
high etch rate	NF_3	600		> 10	spikes
	NF_3/10% O_2	830		> 10	spikes
	SF_6/20% O_2	450		> 10	N
	CF_4/20% O_2	350		7 to 8	N
	CHF_3/60 to 80% O_2	350 to 370		3 to 4	N
	$CBrF_3$/70 to 80% O_2	350 to 400[b])			
etch aspect ratio	NF_3	600		15	spikes
	NF_3/10% O_2	830		> 10	spikes
	SF_6/20% O_2	450		> 10	N
residue-free non-metallic electrode	one can use all of the conditions given above				Y
H_2 additive (Fig. 10b and 11)	NF_3/ >50% > O_2	40 to 150		3 to 4	Y
	SF_6/ >10% O_2	50 to 200		3 to 4	Y
	CF_4/0 to 90% O_2	40 to 180	2	3 to 4	Y
	CHF_3/0 to 90% O_2	50 to 350	2	3 to 4	Y
fluorinated mixtures	CF_4/ >75% CHF_3	100 to 150		3 to 4	Y
	NF_3/ >95% CHF_3	150			Y

[a]) Y: Yes; N: No.
[b]) Poly-SiC.

gate–drain (L_D) are given as 0.7, 0.3, and 0.8 μm, respectively. We have shown earlier that average etch steps of the order of ≈1.5 μm can be achieved in fluorinated mixture plasmas [82]. With an expected aspect ratio of ≈3, the lateral etch resulting while etching through the 0.15 μm thick n^+ layer is only 0.05. The n^+ source and drain islands can therefore be readily patterned under residue-free conditions.

In addition to the high speed MESFET device, several other devices [114], such as UMOS, thyristor, heterojunction bipolar transistor (HBT), p–n diode, double diffusion MOS (DMOS), insulated gate transitor (IGT), and MOS capacitors are reported with promising electrical performance. The corresponding device structures are shown in Fig. 30b to h, respectively. For example, UMOS, HBT, and thyristor strictly require residue-free etching for subsequent metal contact process. For MOS devices, the critical issue is to improve the interface quality between SiO_2 and SiC. However, a high etch rate is required to minimize the cost, i.e. increase the throughput. The various etching requirements are dependent on the specific device structure. High etch rates and highly anisotropic profiles are usually necessary for patterning of most of the devices. In the past, we have reported on the reactive ion etching of SiC by discussing the key issues such as selectivity, surface morphology, etch aspect ratio, and etch rate. These key etching issues and etching results for various processes are outlined in Table 2 for 3C-SiC.

Information on the etching of hexagonal (4H and 6H) SiC is summarized in Table 1. Often a trade-off between a variety of requirements is needed.

Interestingly, the residues observed on the etched regions in SiC are similar to those found on Si and attributed to electrode metal contamination [89] when it was etched in pure CF_4 plasma. With H_2 additive in the CF_4 plasma, the residues on the Si etch field were removed [73, 75]. This indicates that the explanation of surface roughening mechanism by attribution to the "micromasking effect" is correct. Since residue-free etching was obtained in Si etching with H_2 additive as well, the mechanism of "etching enhancement of carbon-rich surface" that we proposed for SiC etching in RIE may in fact not be a dominant process parameter during the etching of SiC. Si etching results indicate that gas phase reaction of volatile compounds plays an extremely important role in removing the metal contamination. This mechanism [90] during the Si residue-free etching results in a lower etch rate with the CF_4/H_2 mixture. For etching SiC, however, one can easily find a residue free process resulting in etch rates that are comparable to that resulting in residues. For example, in Fig. 9a, within the shadowed rectangular residue-free region, one finds similar etch rate with (SF_6/90% CHF_3) and without (CF_5/ > 75% CHF_3 and NF_3/ > 95% CHF_3) residues. However, several side-effects may be encountered. For example when H_2 is used as an additive to obtain a residue-free process, it may be implanted into the etched surface resulting in deactivated dopants (thus lowering the surface doping concentration). H_2 may also lead to increased polymer generation, it often affects the etch rate, and results in safety issues (particularly when used eith O_2) during the process.

9. Current Issues and Future Directions

Nearly all plasma processes create damage to the semiconductor materials. Non-uniform plasma may develop lateral currents which result in gate dielectric damage (charging damage) [115 to 118] in the fabrication of Si CMOS ULSI device. The damage itself could also be a part of the overall etching mechanism, such as damage induced chemical reaction (see Section 2). Not only do the charge particles (ions) create this damage, but also high energy photons may produce thin damage layers. For example, when high energy electrons are swept away from the plasma zone and collide with the side walls of the chamber, they may create potentially damaging high energy X-ray [119, 120] and ultraviolet [121] photons. As shown in Fig. 29 [56], plasma etching damage of SiC has been observed by measuring the leakage current in SiC Schottky diodes: the higher the level of damage, the higher is the leakage current. RIE results in higher damage because of the high self-induced bias. It has no control over this bias which is almost fixed for a given system and input rf power. Unlike RIE, high density plasma sources (such as ECR plasma) usually have low plasma potential (< 50 V) so that ion bombardment energy can be controlled at a minimum level of plasma potential. The use of high density plasma sources could therefore minimize the problem of damage due to ion bombardment.

From a production point of view, Si ULSI technology is transferring from a multi-wafer process to a single-wafer process. As the wafer size becomes larger, etching uniformity will become more and more critical in determining the overall etching performance. To increase macro-and micro-etching uniformity [123], substrate temperature and process pressure are the two major factors. To ensure uniform etching of small size samples of SiC in a multi-wafer RIE system, one should control the pressure to reduce ion scat-

tering and maintain laminar etchant gas flow. Various high density plasma sources are better candidates than RIE, which is operated in a lower process pressure and plasma potential.

Highly anisotropic etching profiles are extremely important for patterning most device structures. As the Si device size shrinks, high aspect ratio of the etching profile becomes critical. For SiC, highly anisotropic etching profiles have been obtained in most of the fluorinated oxygen mixtures we investigated, except mixtures with CHF_3. The reasons are directly related to the polymer generation, where the SiC provides the carbon to protect the side wall from being etched. In mixtures of CHF_3 and H_2, short-range prograde etching profiles were obtained, because of additional polymer deposition in the etched area. On the other hand, a residue-free etching process is obtained with CHF_3/H_2 without the need for covering the metallic electrode. Another approach is the use of a non-metallic material cover to prevent metal contamination during RIE. In Si etching, teflon and quartz are the two most popular materials used to cover the metal chamber wall. However, a trade-off between the etch rate, the etching profile, the material design for a given reactor chamber wall, and the type of plasma source utilized is required.

10. Summary

In this paper, we have reviewed recent literature on reactive ion etching of SiC in a variety of fluorinated oxygen mixture gases such as CHF_3/O_2, $CBrF_3/O_2$, CF_4/O_2, SF_6/O_2, NF_3/O_2 and fluorinated mixture gases such as CF_4/CHF_3, SF_6/CHF_3, and NF_3/CHF_3 and SF_6/NF_3. The following items have been discussed: 1. basic etching mechanisms; 2. etch rate, etch aspect ratio (depth/width), and ERR; 3. techniques for obtaining residue-free etching (smooth etched surface); 4. techniques for obtaining sub-μm feature etching; 5. recent progress of high density plasma etching of SiC; 6. the limitations of SiC reactive ion etching.

Acknowledgements The authors would like to acknowledge the support of this work at the University of Cincinnati by the Edison Materials Technology Center, NASA Lewis Research Center, and Wright Patterson Air Force Base. One of us (A.J.S.) would like to acknowledge the early support and encouragement in this direction by Dr. David Nelson.

References

[1] W. F. Knippenberg, Philips Res. Rep. **18**, 161 (1963).
[2] Cree Research, Inc., Durham, NC 27713, USA.
[3] P. G. Neudeck and J. A. Powell, IEEE Electron Device Lett. **15**, 63 (1994).
[4] J. A. Powell, L. G. Matus, and M. A. Kuczmarski, J. Electrochem. Soc. **134**, 46 (1987).
[5] A. J. Steckl and J. P. Li, IEEE Trans. Electron Devices **39**, 2672 (1988).
[6] A. J. Steckl, C. Yuan, J. P. Li, and M. J. Loboda, Appl. Phys. Lett. **63**, 3347 (1993).
[7] C. Yuan, A. J. Steckl, and M. J. Loboda, Appl. Phys. Lett. **64**, 3000 (1994).
[8] J. A. Powell and L. G. Matus, Springer Proc. Phys. **34**, 2 (1989).
[9] J. A. Powell, P. G. Neudeck, L. G. Matus, and J. B. Petit, Mater. Res. Soc. Symp. Proc. **242**, 495 (1991).
[10] R. J. Trew, J.-B. Yan, and P. M. Mock, Proc. IEEE **79**, 598 (1991).
[11] R. F. Davis, G. Kelner, M. Shur, J. W. Palmour, and J. A. Edmond, Proc. IEEE **79**, 677 (1991).

[12] H. Matsunami, Springer Proc. Phys. **71**, 3 (1992).
[13] M. Bhatnagar and B. J. Baliga, IEEE Trans. Electron Devices **40**, 645 (1993).
[14] C. E. Weitzel, J. W. Palmour, C. H. Carter, Jr., and K. Nordquist, IEEE Electron Device Lett. **15**, 406 (1994).
[15] J. W. Palmour, C. E. Weitzel, K. Nordquist, and C. H. Carter, Jr., Inst. Phys. Conf. Ser. No. 137, Chap. 6, 495 (1993).
[16] J. W. Palmour, H. S. Kong, and R. F. Davis, J. Appl. Phys. **64**, 2168 (1988).
[17] D. M. Brown, E. Downey, and M. Ghezzo, Solid State Electronics **39**, 1531 (1996).
[18] V. A. Dimitriev, M. E. Levinshtein, S. N. Vainshtein, and V. E. Chelnokov, Electronics Lett. **24**, 1031 (1988).
[19] J. W. Palmour, J. A. Edmond, H. S. Kong, and C. H. Carter, Jr., Inst. Phys. Conf. Ser. No. 137, Chap. 6, 499 (1993).
[20] W. Xie, J. A. Cooper, Jr., M. R. Melloch, J. W. Palmour, and C. H. Carter, Jr., IEEE Electron Device Lett. **15**, 212 (1994).
[21] C. T. Gardner, J. A. Cooper, Jr., M. R. Melloch, J. W. Palmour, and C. H. Carter, Jr., Appl. Phys. Lett. **61**, 1185 (1992).
[22] T. Sugii, T. Ito, Y. Furumura, M. Doki, F. Mieno, and M. Maeda, J. Electrochem. Soc. **134**, 2545 (1987).
[23] T. Sugii, T. Aoyama, and T. Ito, J. Electrochem. Soc. **136**, 3111 (1989).
[24] T. Sugii, T. Ito, Y. Furumura, M. Doki, F. Mieno, and M. Maeda, IEEE Electron Device Lett. **9**, 87 (1988).
[25] T. Sugii, T. Yamazaki, and T. Ito, IEEE Trans. Electron Devices **37**, 2331 (1990).
[26] S. Nishino, K. Yamazaki, H. Tanaka, and J. Saraie, Springer Proc. Phys. **71**, 411 (1992).
[27] M. Kondo, T. Shiba, Y. Tamaki, and T. Nakamura, J. Electrochem. Soc. **143**, 1949 (1996).
[28] S. T. Sheppard, M. R. Melloch, and J. A. Cooper, IEEE Electron Device Lett. **17**, 4 (1996).
[29] S. Y. Wu and R. B. Campbell, Solid State Electronics **17**, 683 (1974).
[30] S. Yoshida, K. Sasaki, E. Sakuma, S. Misawa, and S. Gonda, Appl. Phys. Lett. **46**, 766 (1985).
[31] S. Yoshida, H. Daimon, M. Yamanaka, E. Sakuma, S. Misawa, and K. Endo, J. Appl. Phys. **60**, 2989 (1986).
[32] N. A. Papanicolaou, A. Christou, and L. Gipe, J. Appl. Phys. **65**, 3526 (1989).
[33] K. Das, H. S. Kong, J. B. Petit, J. W. Bumbarner, and R. F. Davis, J. Electrochem. Soc. **137**, 1958 (1990).
[34] J. R. Waldrop and R. W. Grant, Appl. Phys. Lett. **56**, 557 (1990).
[35] M. Bhatnagar, P. K, McLarty, and B. J. Baliga, IEEE Electron Device Lett. **13**, 501 (1992).
[36] K. Ueno, T. Urushidani, K. Hashimoto, and Y. Seki, IEEE Electron Device Lett. **16**, 331 (1995).
[37] N. Lundberg, M. Östling, P. Tägtström, and U. Jansson, J. Electrochem. Soc. **143**, 1662 (1996).
[38] T. Urushidani, S. Kobayashi, T. Kimoto, and H. Matsunami, Inst. Phys. Conf. Ser. No. 137, Chap. 6, 471 (1993).
[39] A. J. Steckl, J. N. Su, P. H. Yih, C. Yuan, and J. P. Li, Inst. Phys. Conf. Ser. No. 137, Chap. 6, 653 (1993).
[40] A. J. Steckl and J. N. Su, IEEE Electr. Dev. Meet. Tech. Digest 93CH3361-3, 695 (1993).
[41] J. E. Edmond, K. Das, and R. F. Davis, J. Appl. Phys. **63**, 923 (1988).
[42] L. G. Matus, J. A. Powell, and C. S. Salupo, Appl. Phys. Lett. **59**, 1770 (1991).
[43] M. Ghezzo, D. M. Brown, E. Downey, J. Kretchmer, W. Hennessy, D. L. Polla, and H. Bakhru, IEEE Electron Device Lett. **13**, 639 (1992).
[44] M. Ghezzo, D. M. Brown, E. Downey, J. Kretchmer, and J. J. Kopanski, Appl. Phys. Lett. **63**, 1206 (1993).
[45] S. Yaguchi, T. Kimoto, N. Ohyama, and H. Matsunami, Jpn. J. Appl. Phys. **34**, 3036 (1995).
[46] H. Morkoç, S. Strite, G. B. Gao, M. E. Lin, and B. Sverdlov, and M. Burns, J. Appl. Phys. **76**, 1363 (1994).

[47] B. J. Baliga, IEEE Spectrum **32**, 34 (1995).
[48] J. W. Faust, Jr., in: The Etching of SiC, Eds. J. R. O'Connor and J. Smiltens, Pergamon Press, London/Oxford 1960.
[49] J. S. Shor and R. M. Osgood, and A. D. Kutz, Appl. Phys. Lett. **60**, 1001 (1992).
[50] J. S. Shor and A. D. Kutz, J. Electrochem. Soc. **141**, 778 (1994).
[51] Y. Hibi, Y. Enomoto, K. Kikuchi, and N. Shikata, Appl. Phys. Lett. **66**, 817 (1995).
[52] J. Sugiura, W. J. Lu, K. C. Cadien, and A. J. Steckl, J. Vacuum Sci. Technol. B **4**, 349 (1986).
[53] W.-S. Pan and A. J. Steckl, J. Electrochem. Soc. **137**, 212 (1990).
[54] E. Niemann, A. Boos, and D. Leidich, Inst. Phys. Conf. Ser. No. 137, Chap. 7, 695 (1993).
[55] J. R. Flemish, K. Xie, and J. H. Zhao, Appl. Phys. Lett. **64**, 2315 (1994).
[56] K. Xie, J. R. Flemish, J. H. Zhao, W. R. Buchwald, and L. Casas, Appl. Phys. Lett. **67**, 368 (1995).
[57] H. F. Winters, J. Appl. Phys. **49**, 5165 (1978).
[58] J. W. Coburn and H. F. Winters, J. Vacuum Sci. Technol. **16**, 391 (1979).
[59] H. F. Winters, J. W. Coburn, and T. J. Chuang, J. Vacuum Sci. Technol. B **1**, 469 (1983).
[60] D. L. Flamm and G. K. Herb, in: Plasma Etching: An Introduction, Eds. D. M. Manos and D. L. Flamm, Chap. 1, Academic Press, New York 1989.
[61] J. W. Coburn and E. Kay, IBM J. Res. Develop. **23**, 33 (1979).
[62] T. M. Mayer and R. A. Barker, J. Vacuum Sci. Technol. **21**, 757 (1982).
[63] D. L. Flamm, V. M. Donelly, and J. A. Mucha, J. Appl. Phys. **52**, 3633 (1981).
[64] C. J. Mogab, A. C. Adams, and D. L. Flamm, J. Appl. Phys. **49**, 3796 (1978).
[65] D. L. Flamm, see [60] (Chap. 2).
[66] G. W. Grynkewich and J. N. Helbertin, in: Handbook of Multilevel Metallization for Integrated Circuits, Eds. S. R. Wilson, C. J. Tracy, and J. L. Freeman, Jr., Chap. 7, Noyes Publication, New Jersey 1993.
[67] J. W. Palmour, R. F. Davis, P. Astell-Burt, and P. Blackborow, Mater. Res. Soc. Symp. Proc. **76**, 185 (1987).
[68] R. Legtenberg, H. Jansen, M. de Boer, and M. Elwenspoek, J. Electrochem. Soc. **142**, 2020 (1995).
[69] T. Syan, B. J. Baliga, and R. W. Hamaker, J. Electrochem. Soc. **138**, 3076 (1991).
[70] J. W. Palmour, R. F. Davis, T. W. Wallett, and K. B. Bhasin, J. Vacuum Sci. Technol. A **4**, 590 (1986).
[71] J. W. Coburn and M. Chen, J. Appl. Phys. **51**, 3134 (1980).
[72] R. Padiyath, R. L. Wright, M. I. Chaudhry, and S. V. Babu, Appl. Phys. Lett. **58**, 1053 (1991).
[73] P. H. Yih and A. J. Steckl, J. Electrochem. Soc. **140**, 1813 (1993).
[74] J. Wu, J. D. Parsons, and D. R. Evans, J. Electrochem. Soc. **142**, 669 (1995).
[75] P. H. Yih and A. J. Steckl, J. Electrochem. Soc. **142**, 312 (1995).
[76] R. Wolf and R. Helbig, J. Electrochem. Soc. **143**, 1037 (1996).
[77] G. Kelner, S. C. Binari, and P. H. Klein, J. Electrochem. Soc. **134**, 253 (1987).
[78] J. B. Casady, E. D. Luckowski, M. Bozack, D. Sheridan, R. W. Johnson, and J. R. Williams, J. Electrochem. Soc. **143**, 1750 (1996).
[79] B. P. Luther, J. Ruzyllo, and D. L. Miller, Appl. Phys. Lett. **63**, 171 (1993).
[80] N. J. Ianno, K. E. Greenberg, and J. T. Verdeyen, J. Electrochem. Soc. **128**, 2174 (1981).
[81] D. R. Sparks, J. Electrochem. Soc. **139**, 1736 (1992).
[82] P. H. Yih and A. J. Steckl, J. Electrochem. Soc. **142**, 2853 (1995).
[83] P. G. Neudeck, D. J. Larkin, J. E. Starr, J. A. Powell, C. S. Salupo, and L. G. Matus, IEEE Electron Device Lett. **14**, 136 (1993).
[84] H. Park, K. Kwon, and J. Lee, J. App. Phys. **76**, 4596 (1994).
[85] S. Dohmae, K. Shibahara, S. Nishino and H. Matsunami, Japan. J. Appl. Phys. **24**, L873 (1985).
[86] M. Kothandaraman, D. Alok, and B. J. Baliga, J. Electronic Mater. **25**, 875 (1996).
[87] F. Lanois, P. Lassagne, D. Planson, and M. L. Locatelli, Appl. Phys. Lett. **69**, 236 (1996).

[88] J. R. Flemish and K. Xie, J. Electrochem. Soc. **143**, 2620 (1996).
[89] A. J. Steckl and P. H. Yih, Appl. Phys. Lett. **60**, 1966 (1992).
[90] L. M. Ephrath and R. S. Bennett, J. Electrochem. Soc. **129**, 1822 (1982).
[91] M. Valente and G. Queirolo, J. Electrochem. Soc. **131**, 1132 (1984).
[92] J. Kaindl, S. Sotier, and G. Franz, J. Electrochem. Soc. **142**, 2418 (1995).
[93] F. Gendron, L. M. Porter, C. Porte, and E. Bringuier, Appl. Phys. Lett. **67**, 1253 (1995).
[94] S. J. Fonash, J. Electrochem. Soc. **137**, 3885 (1990).
[95] G. S. Orehrlein, R. M. Tromp, Y. H. Lee, and E. J. Petrillo, Appl. Phys. Lett. **45**, 420 (1984).
[96] S. Oda, J. Noda, and M. Matsumura, Jpn. J. Appl. Phys. **28**, L1860 (1989).
[97] J. B. Carter, J. P. Holland, E. Peltzer, B. Richardson, E. Bogle, H. T. Nguyen, Y. Melaku, D. Gates, and M. Ben-Dor, J. Vacuum Sci. Technol. A **11**, 1301 (1993).
[98] R. W. Boswell and R. K. Porteous, Appl. Phys. Lett. **50**, 1130 (1987).
[99] A. J. Perry and R. W. Boswell, Appl. Phys. Lett. **55**, 148 (1989).
[100] R. W. Boswell, A. J. Perry, and M. Emami, J. Vacuum Sci. Technol. A **7**, 3345 (1989).
[101] A. J. Perry, D. Vender, and R. W. Boswell, J. Vacuum Sci. Technol. B **9**, 310 (1991).
[102] J. M. Cook, D. E. Ibbotson, and D. L. Flamm, J. Vacuum Sci. Technol. B **8**, 1 (1990).
[103] J. M. Cook, D. E. Ibbotson, P. D. Foo, and D. L. Flamm, J. Vacuum Sci. Technol. A **8**, 1820 (1990).
[104] Lam Research Corporation, Technical Note TN-003 (1992).
[105] G. Chevalier and F. F. Chen, J. Vacuum Sci. Technol. A **10**, 1389 (1992).
[106] R. W. Boswell, Plasma Physics and Controlled Fusion **26**, 1147 (1984).
[107] D. L. Flamm, D. E. Ibbotson, and W. L. Johnson, US Patent No. 4,918,031 (1990).
[108] I. Tepermeister, N. Blayo, F. P. Klemens, D. E. Ibbotson, R. A. Gottscho, J. T. C. Lee, and H. H. Sawin, J. Vacuum Sci. Technol. B **12**, 2310 (1994).
[109] I. Tepermeister, D. E. Ibbotson, and J. T. Lee, and H. H. Sawin, J. Vacuum Sci. Technol. B **12**, 2322 (1994).
[110] G. W. Gibson, Jr., H. H. Sawin, I. Tepermeister, D. E. Ibbotson, and J. T. C. Lee, J. Vacuum Sci. Technol. B **12**, 2333 (1994).
[111] N. Blayo, I. Tepermeister, J. L. Benton, G. S. Higashi, T. Boone, A. Onuoha, F. P. Klemens, D. E. Ibbotson, J. T. C. Lee, and H. H. Sawin, J. Vacuum Sci. Technol. B **12**, 1340 (1994).
[112] R. A. Gottscho, C. W. Jurgensen, and D. J. Vitkavage, J. Vacuum Sci. Technol. B **2133**, 10 (1992).
[113] P. G. Neudeck, J. Electronic Mater. **24**, 283 (1995).
[114] B. J. Baliga, in: Modern Power Devices, John Wiley & Sons, New York 1987.
[115] D. J. DiMaria, L. M. Ephrath, and D. R. Young, J. Appl. Phys. **50**, 4015 (1979).
[116] L. M. Ephrath and D. J. DiMaria, Solid State Technol. 182 (April 1981).
[117] C. T. Gabriel and J. P. McVittie, Solid State Technol. 81 (June 1992).
[118] C. T. Gabriel and Y. Melaku, J. Vacuum Sci. Technol. B **12**, 454 (1994).
[119] T. J. Castagna, J. L. Shohet, K. A. Ashitani, and N. Hershkowitz, J. Vacuum Sci. Technol. A **10**, 1325 (1992).
[120] T. J. Castagna, J. L. Shohet, D. D. Denton, and N. Hershkowitz, Appl. Phys. Lett. **60**, 2856 (1992).
[121] D. A. Buchanan and G. Fortuño-Wiltshire, J. Vacuum Sci. Technol. A **9**, 804 (1991).
[122] K. P. Giapis, G. R. Scheller, W. S. Hobson, R. A. Gottscho, and Y. H. Lee, Appl. Phys. Lett. **57**, 983 (1990).